

Cite this: *Digital Discovery*, 2025, 4, 1794

# Assessing data-driven predictions of band gap and electrical conductivity for transparent conducting materials†

Federico Ottomano,<sup>ID</sup><sup>a</sup> John Y. Goulermas,<sup>‡</sup><sup>a</sup> Vladimir Gusev,<sup>ID</sup><sup>ab</sup> Rahul Savani,<sup>ID</sup><sup>\*ac</sup> Michael W. Gaultois,<sup>ID</sup><sup>b</sup> Troy D. Manning,<sup>ID</sup><sup>b</sup> Hai Lin,<sup>ID</sup><sup>b</sup> Teresa Partida Manzanera,<sup>ID</sup><sup>b</sup> Emmeline G. Poole,<sup>b</sup> Matthew S. Dyer,<sup>ID</sup><sup>b</sup> John B. Claridge,<sup>b</sup> Jon Alaria,<sup>bd</sup> Luke M. Daniels,<sup>ID</sup><sup>b</sup> Su Varma,<sup>e</sup> David Rimmer,<sup>e</sup> Kevin Sanderson<sup>e</sup> and Matthew J. Rosseinsky<sup>ID</sup><sup>\*b</sup>

Machine Learning (ML) has offered innovative perspectives for accelerating the discovery of new functional materials, leveraging the increasing availability of material databases. Despite the promising advances, data-driven methods face constraints imposed by the quantity and quality of available data. Moreover, ML is often employed in tandem with simulated datasets originating from density functional theory (DFT), and assessed through in-sample evaluation schemes. This scenario raises questions about the practical utility of ML in uncovering new and significant material classes for industrial applications. Here, we propose a data-driven framework aimed at accelerating the discovery of new *transparent conducting materials* (TCMs), an important category of semiconductors with a wide range of applications. To mitigate the shortage of available data, we create and validate unique experimental databases, comprising several examples of existing TCMs. We assess state-of-the-art (SOTA) ML models for property prediction from the stoichiometry alone. We propose a bespoke evaluation scheme to provide empirical evidence on the ability of ML to uncover new, previously unseen materials of interest. We test our approach on a list of 55 compositions containing typical elements of known TCMs. Although our study indicates that ML tends to identify new TCMs compositionally similar to those in the training data, we empirically demonstrate that it can highlight material candidates that may have been previously overlooked, offering a systematic approach to identify materials that are likely to display TCMs characteristics.

Received 9th January 2025  
Accepted 9th May 2025

DOI: 10.1039/d5dd00010f

rsc.li/digitaldiscovery

## 1 Introduction

Data-driven approaches have proposed a valuable change of perspective in the discovery of new functional materials, assisting traditional methods based on experimental investigation and density functional theory (DFT) calculations.<sup>1,2</sup> This has been made possible by the consistent growth of available material repositories (Materials Project,<sup>3</sup> Materials Platform for Data Science,<sup>4</sup> Open Quantum Materials Database,<sup>5</sup> etc.). In recent years, computational methods driven by Machine Learning (ML)

have proven effective in accelerating the exploration of the chemical space, assisting in the identification of dielectric materials,<sup>6</sup> nickel-based superalloys<sup>7</sup> and superhard materials.<sup>8</sup> Despite the broad perspectives opened up by data-driven methods, the horizon of available properties to leverage ML towards the discovery of specific material classes is still quite narrow due to the scarcity and dispersity of available data to train ML models. Many data-driven approaches are based on computed data and thus subject to the approximations and limitations of the calculation themselves. Experimental data are generally not available at scale. Industrial applications frequently require *exceptional* compounds,<sup>9</sup> often exhibiting a counterintuitive combination of two or more chemical properties. This poses significant challenges to current data-driven frameworks, as conventional material databases may lack the necessary information to effectively guide ML in discovering materials tailored at specific applications.

Transparent conducting materials (TCMs) fully exemplify the category of exceptional compounds. These represent a class of semiconductors showing simultaneously high electrical conductivity, and low absorption in the range of visible light. This unique

<sup>a</sup>Department of Computer Science, University of Liverpool, Ashton Street, L69 3BX Liverpool, UK. E-mail: rahul.savani@liverpool.ac.uk

<sup>b</sup>Materials Innovation Factory, Department of Chemistry, University of Liverpool, 51 Oxford Street, L7 3NY Liverpool, UK. E-mail: rosseinsky@liverpool.ac.uk

<sup>c</sup>The Alan Turing Institute, British Library, 96 Euston Rd., London NW1, UK

<sup>d</sup>Department of Physics, University of Liverpool, Oxford Street, Liverpool L69 7ZE, UK

<sup>e</sup>Pilkington Technology Management Ltd., NSG Group European Technical Centre Hall Lane, Lathom Ormskirk LA0 5UF, UK

† Electronic supplementary information (ESI) available. See DOI: <https://doi.org/10.1039/d5dd00010f>

‡ Deceased in May 2022.



behaviour is often enforced in practice by a process known as *doping*, where additional components are introduced into an intrinsic semiconductor to modulate its optoelectronic properties. Conventional transparent conductors are typically achieved by doping metal oxide semiconductors like  $\text{In}_2\text{O}_3$ ,  $\text{SnO}_2$ ,  $\text{CdO}$  and  $\text{ZnO}$ . Among various classes of TCMs, tin-doped indium oxide (ITO) stands out as the most common one typically used in high value applications such as displays due to the scarcity of indium, while fluorine-doped tin oxide (FTO) has been widely adopted in larger area applications such as solar control glazing and transparent electrodes for solar cells.<sup>10</sup> Although the existing set of TCMs currently addresses the demands imposed by modern optoelectronic applications, the scarcity of raw materials, together with the high costs of vapour deposition techniques, drive researchers to look for alternative solutions.<sup>11,12</sup> Previous literature using ML in the TCMs field has investigated the optimization of existing semiconductors,<sup>13</sup> or focused on well-defined phase-fields,<sup>14,15</sup> and progress has been hindered due to the absence of adequate datasets of experimental optoelectronic properties.

In this work, we propose a data-driven framework to accelerate the discovery of new TCMs. To address the shortage of available data, we create and validate databases of chemical formulas reporting experimental room-temperature conductivity and band gap measurements. We utilize the obtained data to train state-of-the-art (SOTA) ML models that leverage the stoichiometry of input materials, taking into account that composition and the presence of dopants are important for conductivity and band gap, given the typical absence of structural information in materials discovery tasks. Furthermore, we assess the performance of trained models using a custom evaluation framework, designed to determine whether ML can identify previously unseen classes of TCMs. To test the proposed framework, we further utilize a list of 55 experimentally-reported chemical compositions sourced from entries across MPDS,<sup>4</sup> Pearson,<sup>16</sup> and ICSD databases.<sup>17</sup> We use this list to empirically demonstrate the effectiveness of ML in accelerating the identification of new materials that are likely to display TCMs characteristics. The main contributions of this study can be summarized as follows:

- We create two datasets of experimentally-reported optoelectronic properties, (1) a dataset of electrical conductivity is collated and curated from data residing in the MPDS and (2) we augment a published band gap dataset. Both datasets serve as a foundation for training ML models aimed at the identification of TCMs.
- We evaluate SOTA ML models for property-prediction on the proposed experimental datasets.
- We empirically measure the ability of ML models to identify new classes of TCMs through a bespoke evaluation method.
- We compile a list of 55 compositions across various databases and we empirically demonstrate the potential of ML in accelerating the identification of materials that are likely to exhibit TCMs characteristics.

## 2 Related work

### 2.1 Computationally-guided search for new TCMs

DFT has primarily enabled a computational exploration of various material classes, including TCMs. Notably, Woods-

Robinson *et al.*<sup>13</sup> curated an experimental dataset comprising 74 bulk structures of well-known TCMs with the goal of computing a set of DFT-based descriptors that would capture essential features of these materials for computational screening purposes. Hautier *et al.*<sup>18</sup> employed a high-throughput computational approach to identify oxides with low electron effective mass. They also assessed the band gap of the most promising candidates and proposed potentially novel n-type transparent conducting oxides. The increasing accessibility of materials data has also facilitated data-driven frameworks for ML-guided search for new materials. Sun *et al.*<sup>19</sup> conducted a study that explored the application of ML to predict new TCMs. They utilized data on formation energy and band gap obtained from a Kaggle competition focused on TCMs discovery.<sup>19</sup> Despite the promises established by computational modelling, challenges such as high computational cost and systematic errors in DFT-based approaches, along with the scarcity of suitable datasets in the realm of ML, have posed important obstacles to the search for new such materials.

### 2.2 Data-driven identification of optoelectronic properties

Electronic transport and optical data on semiconductors have been gathered and evaluated in the context of thermoelectrics<sup>20,21</sup> and of band gap.<sup>22,23</sup> Studies have then evaluated different ML approaches in combination with data extracted from the University of California Santa Barbara (UCSB) dataset to predict the electrical conductivity of materials.<sup>24,25</sup> Furthermore, DFT-calculated datasets for electron transport properties have also been proposed<sup>26–29</sup> and utilized for different tasks ranging from data visualization, to ML property prediction. The availability of experimental datasets has remained rather limited,<sup>21,30–32</sup> with most available datasets reaching the order of  $\sim 10^2$  entries. Furthermore, experimental data often encompass minimal chemical diversity, primarily due to the difficulties in obtaining reliable measurements. These two crucial issues (limited datasets size and narrow chemical diversity) heavily limit the application of data-driven methods for the prediction of electronic properties. In the case of band gap, the extensive availability of entries derived from DFT calculations<sup>3,5,33</sup> has, in part, mitigated the problem of data scarcity, specifically because this property is more feasible to theoretical simulations compared to electron transport properties. However, significant challenges persist in the prediction of experimental band gaps due to the underestimation of band gaps calculated using the high-throughput DFT approaches of large databases<sup>34</sup> and imbalance between metals and non-metals in the available datasets.<sup>5</sup>

## 3 Databases overview

A well-established figure of merit for TCMs can be identified as the ratio of electrical conductivity ( $\sigma$ ) to the optical absorption coefficient ( $\alpha$ ):<sup>35</sup>

$$\varphi_{\text{TCM}} = \frac{\sigma}{\alpha}. \quad (1)$$



A well-performing TCM should combine high electrical conductivity with low absorption of visible light. Therefore, to accommodate  $\varphi_{\text{TCM}}$  within a data-driven perspective, it would be necessary to rely on abundance of data in terms of  $\sigma$  and  $\alpha$ . Typically, datasets containing these properties are scarce and fragmented across numerous sources in the literature. To address the limitation of optical property data, we adopt the band gap ( $E_g$ ) as a proxy for optical transparency, motivated by the abundance of this information in the existing literature.<sup>3,5</sup> The band gap is a crucial parameter that influences materials' optical properties. A material with a band gap exceeding the energy of visible light (approximately 3 eV) appears generally transparent, as photons within this range lack the energy to excite electrons across the band gap. Thus, by choosing materials with band gaps greater than 3 eV, we can identify materials that are likely to exhibit transparency in the visible spectrum. To enable a ML approach, we have created and validated two experimental datasets of room-temperature conductivity and band gap measurements, to be used as foundation for training SOTA ML models for the discovery of new TCMs. Below, we detail the creation of these databases, a key contribution of this work. Both datasets were tailored to remove unphysical entries by expert assessment and to ensure that a wide range of chemistries were included, resulting in datasets well-balanced between metals and non-metals as discussed below.

### 3.1 Electrical conductivity dataset

The electrical conductivity dataset was constructed using two primary data sources. Initially, data on conductivity and resistivity, along with associated chemical formulas, were gathered from the Materials Platform for Data Science (MPDS),<sup>4</sup> with 38 068 entries available as of December 2024. This source was supplemented with the UCSB dataset<sup>21</sup> (1794 entries), which provides a range of experimental thermoelectric properties, including electrical conductivity. In total, we compiled a raw dataset comprising 39 862 material entries with associated conductivity measurements at various temperatures. Several preprocessing steps were conducted on the raw data. Initially, we excluded all pure elements and noble gases and selected all chemical formulas reported within a window of room temperature ( $298 \pm 5$  K), reducing the dataset to 14 307 entries. Given the experimental nature of utilized data, it is common to encounter several material entries where different measurements are documented for identical chemical formulas at the same temperatures. This variance is inherently linked to the different experimental conditions under which these measurements were conducted. To process raw data in view of statistical estimation, we initially considered the distributions of measurements corresponding to duplicated chemical formulas, discarding those groups associated to a standard deviation exceeding  $10 \text{ S cm}^{-1}$ .

Furthermore, we excluded entries with conductivity measurements falling outside of 4 standard deviations from the mean, resulting in a processed dataset containing 8034 material entries. At this stage, we performed a meticulous validation, which involved a line-by-line review of the obtained data by domain experts, referring back to the original literature on

suspicious entries, to ensure the accuracy of the reported conductivity measurements, alongside the correctness of the corresponding chemical formulas. To facilitate the validation process, automated nonsense-detection strategies were implemented to systematically identify anomalous conductivity measurements associated to the reported material entries. This involved inferring the oxidation states of the chemical elements in each composition, to ensure the feasibility of different chemical species, in accordance with their corresponding conductivity measurements. First, Comgen<sup>36</sup> was used to infer the oxidation states of chemical elements in each composition. These were used to verify the feasibility of the chemical species in the composition, in accordance with the reported conductivity measurement. For example, closed-shell, *i.e.* fully stoichiometric and undoped, oxides are expected to exhibit low conductivities. Therefore, reported entries corresponding to closed-shell oxides with a conductivity higher than a threshold set to  $10^{-6} \text{ S cm}^{-1}$  were automatically flagged by the nonsense-detection tool for further expert consideration. Additionally, we incorporated experimental conductivities for several chemical families that were absent, such as the alkaline earth oxides, binary and ternary oxides including materials selected to represent each integer transition metal oxidation state as far as available data allow, as well as known TCMs (reported in Table 1). We end up with a final, validated database comprising 8231 material entries, with a mean  $\bar{x}$  of 1.09 ( $\log_{10} (\text{S cm}^{-1})$ ), a median  $\bar{x}$  of 2.44 ( $\log_{10} (\text{S cm}^{-1})$ ) and an interquartile range (50% of data; materials from the 25th to the 75th percentile of  $\log_{10}(\sigma)$ ) spanning from  $-0.18$  to  $3.60$  ( $\log_{10} (\text{S cm}^{-1})$ ). The data distribution of conductivity dataset is shown on the left of Fig. 1. To understand the distribution of metals and non-metals in our conductivity dataset, we utilize the theoretical notion of minimum metallic conductivity (MMC), as introduced in ref. 37. This indicates a threshold below which materials exhibit semiconductor-like behavior. Thus, compounds with conductivity above this threshold display metallic characteristics, while those below it show a non-metallic behavior. For our analysis, we adopt a threshold value of  $\sigma_{\text{min}} = 10^3 \text{ S cm}^{-1}$ , represented by the purple dotted line in Fig. 1 (left), which has been experimentally observed for many transition metal compounds near the metal-insulator transition.<sup>38</sup> Applying this criterion, we

**Table 1** Various families of TCMs, each with distinct  $N$  representatives associated to a specific doping level (at%). We report the mean ( $\mu$ ) and standard deviation ( $s$ ) related to conductivity and band gap measurements for different families

| TCMs family  | $N$ | $\sigma$ ( $\log_{10} (\text{S cm}^{-1})$ ) ( $\mu \pm s$ ) | $E_g$ (eV) ( $\mu \pm s$ ) |
|--|-----|---|----------------------------|
| SnO <sub>2</sub> : Ga <sup>43</sup>                        | 3   | $2.52 \pm 0.03$   | $3.77 \pm 0.03$            |
| SnO <sub>2</sub> : In <sup>42</sup>                        | 4   | $2.26 \pm 0.75$   | $3.83 \pm 0.09$            |
| SnO <sub>2</sub> : Mn <sup>44</sup>                        | 3   | $2.07 \pm 0.01$   | $4.07 \pm 0.03$            |
| SnO <sub>2</sub> : Ta <sup>45</sup>                        | 3   | $2.52 \pm 0.54$   | $4.16 \pm 0.11$            |
| SnO <sub>2</sub> : Ti <sup>46</sup>                        | 5   | $2.73 \pm 0.06$   | $3.80 \pm 0.06$            |
| SnO <sub>2</sub> : W <sup>47</sup>                         | 4   | $2.23 \pm 0.22$   | $4.23 \pm 0.68$            |
| In <sub>2</sub> O <sub>3</sub> : Sn <sup>50–52</sup> (ITO) | 3   | $2.65 \pm 0.64$   | $3.73 \pm 0.29$            |
| ZnO: Al–Sn <sup>53</sup>                                   | 4   | $2.58 \pm 0.18$   | $3.80 \pm 0.16$            |
| ZnO: Al <sup>48</sup>                                      | 3   | $3.43 \pm 0.57$   | $3.61 \pm 0.05$            |
| ZnO: Ga <sup>49</sup>                                      | 6   | $3.93 \pm 0.29$   | $3.64 \pm 0.05$            |



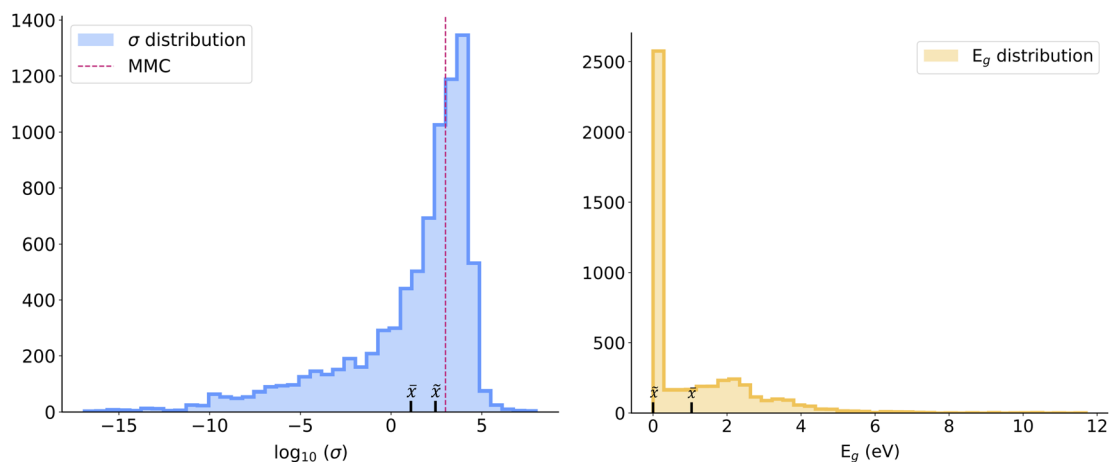


Fig. 1 Data distributions for  $\sigma$  (left) and  $E_g$  (right).  $\bar{x}$  and  $\tilde{x}$  denote the mean and the median, respectively. The purple dotted line on  $\sigma$  distribution indicates the minimum metallic conductivity  $\sigma_{\min} = 10^3$  (S cm<sup>-1</sup>).

identified 3187 metals in the dataset ( $\approx 39\%$ ), and 5044 materials ( $\approx 61\%$ ) exhibiting non-metallic conductivity.

### 3.2 Band gap dataset

The initial band gap data was sourced from a well-known experimental dataset proposed by ref. 22. The original dataset comprises 6354 material entries with experimental band gap measurements determined from optical and transport measurements. Preprocessing steps were applied to the raw data. Specifically, we excluded groups of duplicated formulas with band gap measurements having a standard deviation greater than 0.1 eV. This preprocessing approach is similar to the one used for creating the matbench\_xpt\_gap dataset, available on the Matbench platform.<sup>39</sup> All the entries associated with noble gases and pure elements have been discarded. Additionally, entries with band gap measurements exceeding 4 standard deviations from the mean have been excluded, leading to a processed dataset of 4732 material entries. As in the case of conductivity, the obtained pool of data has been expanded by including experimental band gap measurements of binary and ternary oxides not already in the dataset, along with known TCMS, reported in Table 1. The additional data was taken from the primary literature<sup>40–49</sup> after identifying the gaps in the original dataset. These preprocessing steps resulted in a final dataset comprising 4767 material entries, with a mean  $\bar{x}$  of 1.04 (eV), a median  $\tilde{x}$  of 0.00 (eV), and an interquartile range spanning from 0.00 to 1.93 eV. The data distribution of the band gap dataset is shown on the right in Fig. 1. We observe a balanced representation of metals ( $E_g = 0$ ) and non-metals ( $E_g > 0$ ) in the created dataset. The group of metals comprises 2426 material entries ( $\approx 51\%$ ), while non-metals encompass 2341 entries ( $\approx 49\%$ ).

## 4 Methods

In this section, we introduce both the ML models and the evaluation methods considered in this study.

### 4.1 Representation of stoichiometry for Machine Learning approaches

A central aspect in composition-based ML is selecting suitable representations of input stoichiometry that reflect the underlying chemical principles. Given a compound containing elements  $(a_1, a_2, \dots, a_N) \in \mathbb{A}^N$ , where  $\mathbb{A}$  denotes the (abstract) set of all chemical elements, it is common to consider a mapping  $\mathfrak{F}: \mathbb{A} \rightarrow \mathbb{R}^{d_f}$  that represents a chemical element  $a_i$  with a vector  $\mathbf{c}_i \in \mathbb{R}^{d_f}$ . The choice of  $\mathfrak{F}$  determines the nature of the representation and is often tailored to the ML model being employed. In our study, we utilize two distinct representations: Magpie descriptors<sup>54</sup> and Mat2vec embeddings.<sup>55</sup> Each reflects a different approach to encoding element information, the former being manually crafted, the latter learned from data. To use these element-level features in ML models, a global representation of the compound must be derived. For traditional ML models like linear regression or tree-based algorithms, it is common to construct a composition-based feature vector (CBFV) by aggregating element vectors:

$$\mathbf{v} = \sum_{i=1}^N w_i \mathbf{c}_i, \quad w_i = \frac{n_i}{\sum_{j=1}^N n_j}, \quad (2)$$

where  $n_i$  denotes the number of atoms of element  $a_i$  in the formula, and  $w_i$  represents its fractional contribution. This pooling operation produces a single vector  $\mathbf{v} \in \mathbb{R}^{d_f}$  that represents the entire compound. In our experiments, we apply this aggregation to Magpie descriptors,<sup>54</sup> which are handcrafted vectors ( $d_f = 132$ ) incorporating physical and chemical attributes (e.g. atomic number, electronegativity etc.), along with statistical operations such as mean and standard deviation. In contrast, Mat2vec embeddings<sup>55</sup> are not aggregated *via* CBFV. Instead, they have been used in tandem with attention-based deep learning architectures to learn relationships between the elements in a compound.<sup>56</sup> Mat2vec embeddings are data-driven representations, where each chemical element is assigned to a vector ( $d_f = 200$ ) trained from co-occurrence



patterns in materials science literature. Mat2vec embeddings have proven particularly effective when paired with deep learning models for property prediction.<sup>56,57</sup> This is likely due to the incorporation of a broader material science knowledge learned from scientific literature. As a result, the embeddings can adapt flexibly to specific material–property relationships through nonlinear transformations in neural network models. Specifically, in our experiments we adopt Random Forest (RF)<sup>58</sup> with CBFVs obtained from Magpie descriptors, and CrabNet<sup>56</sup> paired with Mat2vec embeddings.

## 4.2 Models

**4.2.1 Random forest.**<sup>58</sup> A classic ML approach that is well established in the field of materials informatics and has been applied in a variety of tasks, from predicting band gap energy<sup>59</sup> to identifying thermoelectric and mechanical properties.<sup>60,61</sup> The algorithm involves a combination of various weak learners that are trained on resampled versions of the original dataset and with different subsets of features. This has the effect of reducing model variance by decorrelating individual decision trees. In practice, it is commonly used in tandem with materials representations obtained by aggregating attributes from individual elements of the periodic table. These features are typically denominated structure or composition-based feature vectors, given that they are obtained using the stoichiometry alone,<sup>54</sup> or other known attributes from the underlying crystal-line structure.<sup>62</sup>

**4.2.2 CrabNet.**<sup>56</sup> A neural-network architecture based on the paradigm established by transformers.<sup>63</sup> The core idea of these models relies on self-attention, which finds an early application in the field of natural language processing: intuitively, given a sequence (phrase) of  $n$  tokens  $\mathbf{x}_1, \mathbf{x}_2, \dots, \mathbf{x}_n$ , the goal is to learn new, context-aware representations  $\mathbf{y}_1, \mathbf{y}_2, \dots, \mathbf{y}_N$ , with a richer semantic structure. This is achieved by learning attention scores between word pairs within the phrase.

In the context of materials science, the input tokens can be viewed as elements of a chemical composition. Attention scores, computed *via* self-attention, can then be utilized to adjust the overall material representation for predicting a specific property of interest. CrabNet has delivered remarkable outcomes in predicting chemical and physical properties of materials when only the composition is available.<sup>39</sup> It frequently serves as a SOTA model in scenarios where property predictions are solely reliant on the chemical composition of materials.<sup>64–67</sup> For further details regarding the underlying architecture, we refer to the original paper.<sup>56</sup>

## 4.3 Evaluation

In our goal of identifying the constitutive properties of the materials of interest, we stay aligned to previous work<sup>23,24,65,68</sup> and adopt a regression task. In this context, the goal is to train ML models to predict numerical values associated to the corresponding material properties. It is worth mentioning that a classification task may be considered too, directly determining whether the predicted material meets the specified criteria or not and thus falls into the category of TCMs.

However, we argue that adopting a classification approach in this context might sacrifice valuable interpretability. Rather than simply classifying materials as TCMs or non-TCMs, regression models provide continuous numerical predictions for properties like conductivity and band gap. This granularity offers a more precise understanding of each material's performance, allowing us to evaluate how close each material is to meeting the TCM criteria. To assess the performance of trained ML models, we utilize different evaluation schemes: K-fold, a conventional method deeply rooted in statistical learning theory,<sup>69</sup> is commonly employed; additionally, Leave-One-Cluster-Out Cross-Validation (LOCO-CV)<sup>70</sup> stands as an alternative method targeting the assessment of chemical extrapolation, crucial for discovering new materials, absent in the training data. Furthermore, we introduce a third evaluation method designed to offer nuanced interpretability within the task at hand, namely the discovery of novel TCMs. Details outlining each of these methods are provided in the following.

**4.3.1 K-fold.** Validation process involves quantifying the deviation between predictions and real underlying targets, in a portion of the dataset that is held out at training stage. This is typically achieved with a K-fold cross validation, which consists in splitting the original dataset in  $k$  equally-sized folds ( $k = 5$  in this study), and in turn, training the model on  $k - 1$  of these and using the remaining one for evaluation, to have an estimate of the average test error. While K-fold cross-validation is a well-established and commonly used procedure for assessing the performance of ML models, it may not serve as an accurate indicator of their extrapolation capability in the context of materials discovery. The main concern arises from the fact that within a K-fold approach, similar stoichiometries can end up in both training and test data. As a consequence, the model might be provided with a relatively favorable scenario, where it can effortlessly interpolate between known stoichiometries, rather than being truly challenged to extrapolate beyond the observed data. This aspect is intrinsically connected to the redundancy of material datasets,<sup>71,72</sup> which inevitably leads to overestimating the performance of ML models,<sup>73</sup> unless bespoke evaluation schemes are designed to quantify the extrapolation error. This phenomenon can potentially mask any limitations or weaknesses in the models' ability to generalize to new and unseen materials, undermining the overall predictive power in the context of materials discovery.

**4.3.2 LOCO-CV.** While K-fold cross-validation remains valuable for assessing models' performance within the training distribution, it may not fully capture the crucial aspect of extrapolation in any materials discovery task involving ML. In addition to K-fold, we employ a LOCO-CV<sup>70</sup> evaluation scheme. With LOCO, the folds are not randomly generated, but rather constructed by grouping together material families that exhibit chemical similarity. This method provides a more refined evaluation of models' performance by focusing on the ability to generalize to new material groups. For example, one might be interested in assessing the extrapolation power of a ML model in predicting a group of oxides given that this family was unobserved at training stage. Different techniques can be employed to effectively implement this approach: in general,



when featurizing input chemical formulas, the initial step often involves employing the K-means algorithm<sup>74</sup> to generate a pre-determined number of distinct clusters. However, a challenge arises due to the eventual *disparity* in the sizes of material groups, which can introduce excessive variance during the evaluation process. To address this scenario, prior observations have indicated that applying kernel functions to the material representations can promote more equitable cluster sizes and enhance the invariance of the resulting clusters with respect to the chosen representation for the input chemical formulas.<sup>75</sup> Kernels are mathematical functions that transform the input data into a higher-dimensional feature space where better linear separability is possible.<sup>76</sup> To leverage these benefits in our approach, we employ a kernel-based feature transformation before clustering. We utilize RBFSampler from scikit-learn, which approximates the feature map of a radial basis function kernel using random Fourier features. Specifically, the original CBFVs (depicted in eqn (2)) are transformed into high-dimensional representations  $\phi(\mathbf{v})$ , which are then used as input for K-means clustering. The K-means algorithm partitions the dataset into  $k$  clusters by minimizing the within-cluster variance. Given a set of  $M$  transformed feature vectors  $\{\phi(\mathbf{v}_1), \dots, \phi(\mathbf{v}_M)\}$ , the objective is to find cluster centers  $\{\mu_1, \dots, \mu_k\}$  that minimize the sum of squared distances:

$$\arg \min_{\mu_1, \dots, \mu_k} \sum_{j=1}^k \sum_{\phi(\mathbf{v}_i) \in C_j} \|\phi(\mathbf{v}_i) - \mu_j\|^2, \quad (3)$$

where  $C_j$  is the set of feature vectors assigned to cluster  $j$ . The number of clusters  $k$  is a hyperparameter, and we set  $k = 5$  in our experiments.

**4.3.3 Leave-one-TCM-family-out.** In principle, LOCO-CV can be considered as a well-motivated method to evaluate the chemical extrapolation of ML models under consideration. However, the assessment is often limited by the varying sizes of material clusters, which lead to a noisy evaluation and to an increased variance in the assessed metrics. Moreover, it is

common for the data folds generated within a LOCO-CV setting to result from the sequential application of various algorithms, which in turn leads to a limited interpretability regarding the resulting material clusters. To gather empirical evidence regarding the ability of ML to uncover novel compounds for real-world applications, we propose a new evaluation strategy that we denote as *leave-one-TCM-family-out*. This evaluation method aims at providing empirical evidence on whether ML can discover new TCMs, given prior knowledge from known materials. For a comprehensive analysis, we initially gather diverse families of established TCM materials. In Table 1 we present a summary of different material families examined in this study, along with the count of associated representatives and the average values of reported electrical conductivity and band gap measurements. In total, we have compiled 38 examples of established TCMs from the existing literature. Different representatives within the same family reflect different concentrations (at%) of the corresponding dopant element. Drawing insights from the statistics of reported TCMs and from prior scientific knowledge, we establish an identification criterion aimed at understanding whether ML can successfully identify TCM materials: specifically, a TCM will be successfully identified if the corresponding predictions for electrical conductivity and band gap exceed  $10^2 \text{ S cm}^{-1}$  and 3 eV, respectively. Intuitively, we want to investigate whether ML models can discriminate the behavior of doped semiconductors, and detect a significant level of electrical conductivity, even in situations where there exists a non-negligible band gap. In the leave-one-TCM-family-out evaluation scheme, we exclude a specific family of TCMs from the training set, while retaining other representative materials. Importantly, when a cluster of extrinsically doped semiconductors is placed in the test set, the corresponding undoped semiconductor remains in the training set as prior knowledge. For example, all ZnO:Al materials may be placed in the test set while ZnO is retained in the training data. In practice, this assessment seeks to offer

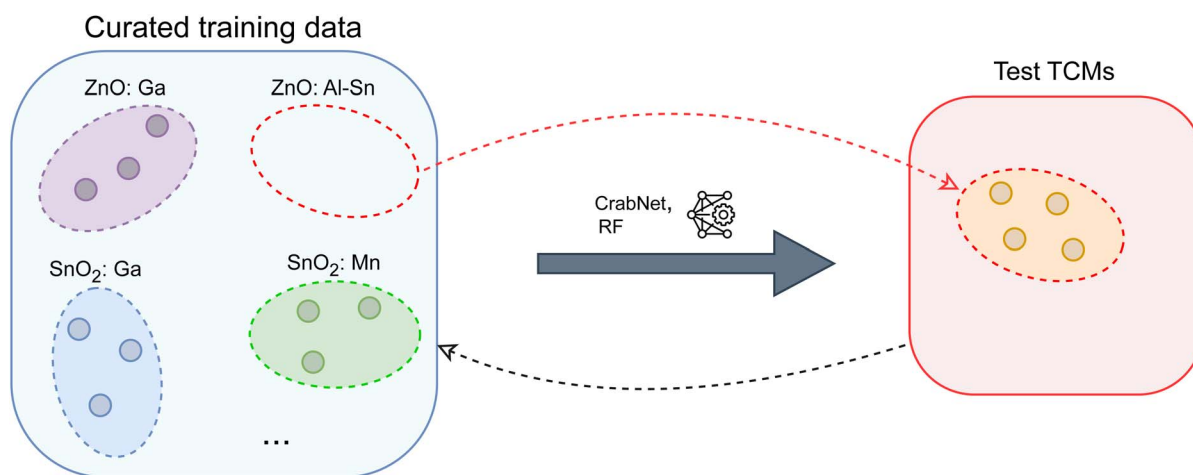


Fig. 2 Schematic representation of the proposed evaluation to simulate the discovery of new TCMs: following an iterative scheme, a specific family of known TCMs is placed in the test set, while ML models are trained on the remaining TCMs within training data. This procedure repeats for each available TCM family.



empirical evidence about the ability of ML to uncover novel material families, leveraging the existing knowledge as a starting point. In practice, we are asking ML models to identify new stoichiometric combinations in the test set previously unobserved at training stage. If one of the TCM families, either SnO<sub>2</sub>: In or In<sub>2</sub>O<sub>3</sub>: Sn, is present in the test set, the other is excluded from training, as they share the same chemical elements, despite representing two different sets of TCMs. To quantify the success rate in the proposed evaluation, we establish a new metric named *family-discovery-rate* (FDR), which considers the percentage of discovered TCMs families by ML, with success defined as the accurate prediction of at least one representative from the overall family, when that family is removed from the training data. We define it as:

$$\text{FDR (\%)} := \frac{N_f^*}{N_f} \times 100, \quad (4)$$

where  $N_f$  represents the total number of families and  $N_f^*$  is the count of correctly predicted families. In Fig. 2, we provide a visual overview of the proposed evaluation scheme.

## 5 Results

Since the primary task can be formulated as a regression problem, we utilize mean absolute error (MAE) and coefficient of determination ( $R^2$ ) as evaluation metrics to assess models' performance. For band gap prediction, CrabNet undergoes pre-training on a dataset of DFT-computed band gaps sourced from the Materials Project.<sup>3</sup> This pre-trained model is then fine-tuned on the curated experimental band gap dataset (results for CrabNet's band gap predictions, shown in Table 3, pertain to this fine-tuned model). During fine-tuning, we choose to retrain

all model weights rather than freezing earlier layers. This approach retains knowledge from the larger DFT dataset while allowing the model to fully adapt to experimental trends. We adopt this transfer learning strategy to help mitigate well-known ML limitations in band gap prediction, which often lead to metallic materials being incorrectly classified as semiconductors or insulators.<sup>6</sup>

### 5.1 kFold & LOCO-CV

In Tables 2 and 3 we report evaluation results for ML prediction on both the properties considered. Fig. 3 illustrates the distinct material clusters obtained for the LOCO-CV evaluation setting, projected onto a two-dimensional space for visualization using Principal Component Analysis (PCA). Specific chemical elements included in each cluster are provided in the ESI.† In Fig. 4, we show parity plots related to the K-fold evaluation scheme.

**5.1.1 Conductivity prediction.** For electrical conductivity, CrabNet and RF yield comparable in-sample results (K-fold), with RF achieving a ~4% higher  $R^2$  than CrabNet, and a slight improvement of MAE, although not statistically significant. Such an outcome is expected, considering the remarkable performance of RF in interpolation tasks (in-sample). This is due to the intrinsic ensemble nature of the algorithm, enabling a good generalization within the range of training data. In the out-of-sample evaluation (LOCO-CV), we observe that differences among models are not statistically significant and are subject to high variability. This primarily stems from the size disparities among various material clusters. Additionally, it is plausible that certain material groups contain crucial chemical information that is missing from the training data. The systematic exclusion of such clusters at training stage may lead

**Table 2** ML models evaluation for electrical conductivity ( $\sigma$ ) prediction ( $\log_{10}$  (S cm<sup>-1</sup>)). Best-performing results are shown in green, while second best-performing are shown in yellow, when there is an overlap in the uncertainty bands. Upward and downward arrows indicate the desired direction for improvement for the corresponding metric

| Model       | kFold              |                    | LOCO-CV            |             |
|-------------|--------------------|--------------------|--------------------|-------------|
|             | MAE ↓              | $R^2$ ↑            | MAE ↓              | $R^2$ ↑     |
| RF + Magpie | <b>1.16 ± 0.05</b> | <b>0.72 ± 0.02</b> | 1.92 ± 0.94        | 0.23 ± 0.25 |
| CrabNet     | 1.18 ± 0.05        | 0.69 ± 0.03        | <b>1.72 ± 0.80</b> | 0.17 ± 0.24 |

**Table 3** ML models evaluation for band gap ( $E_g$ ) prediction (eV). Best-performing results are shown in green, while second best-performing are shown in yellow, when there is an overlap in the uncertainty bands. '—' indicates a negative  $R^2$  score, and thus the failure of the corresponding regression task. Upward and downward arrows indicate the desired direction for improvement for the corresponding metric

| Model       | kFold              |                    | LOCO-CV            |                    |
|-------------|--------------------|--------------------|--------------------|--------------------|
|             | MAE ↓              | $R^2$ ↑            | MAE ↓              | $R^2$ ↑            |
| RF + Magpie | 0.41 ± 0.02        | 0.70 ± 0.03        | 0.86 ± 0.40        | —                  |
| CrabNet     | <b>0.30 ± 0.02</b> | <b>0.73 ± 0.05</b> | <b>0.56 ± 0.32</b> | <b>0.47 ± 0.15</b> |



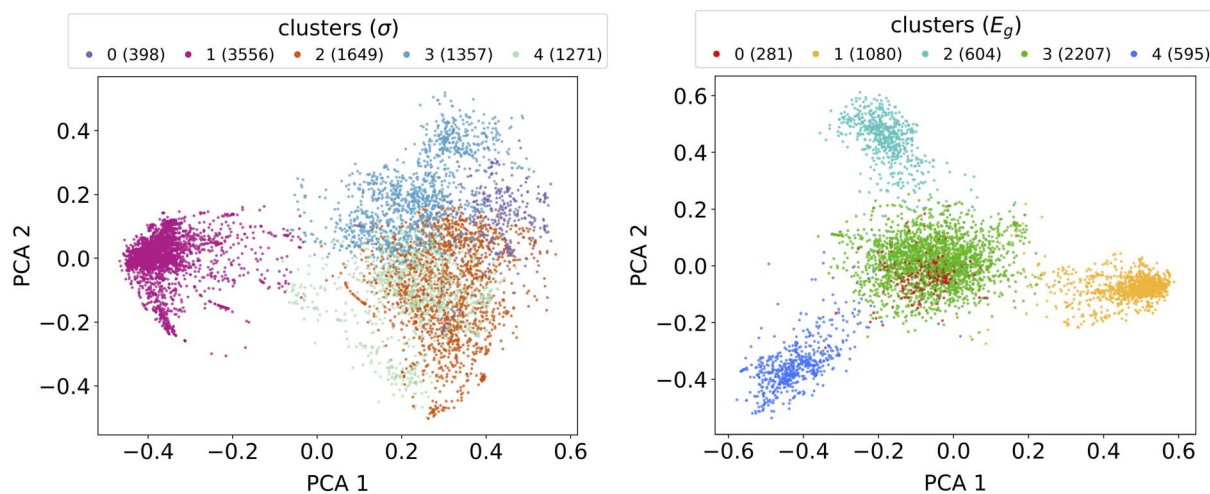


Fig. 3 LOCO-CV material clusters obtained separately for the conductivity dataset (left) and for the band gap dataset (right), projected onto a two-dimensional space for visualization using Principal Component Analysis (PCA). More details on the compositions included in each cluster can be found in the ESI.†

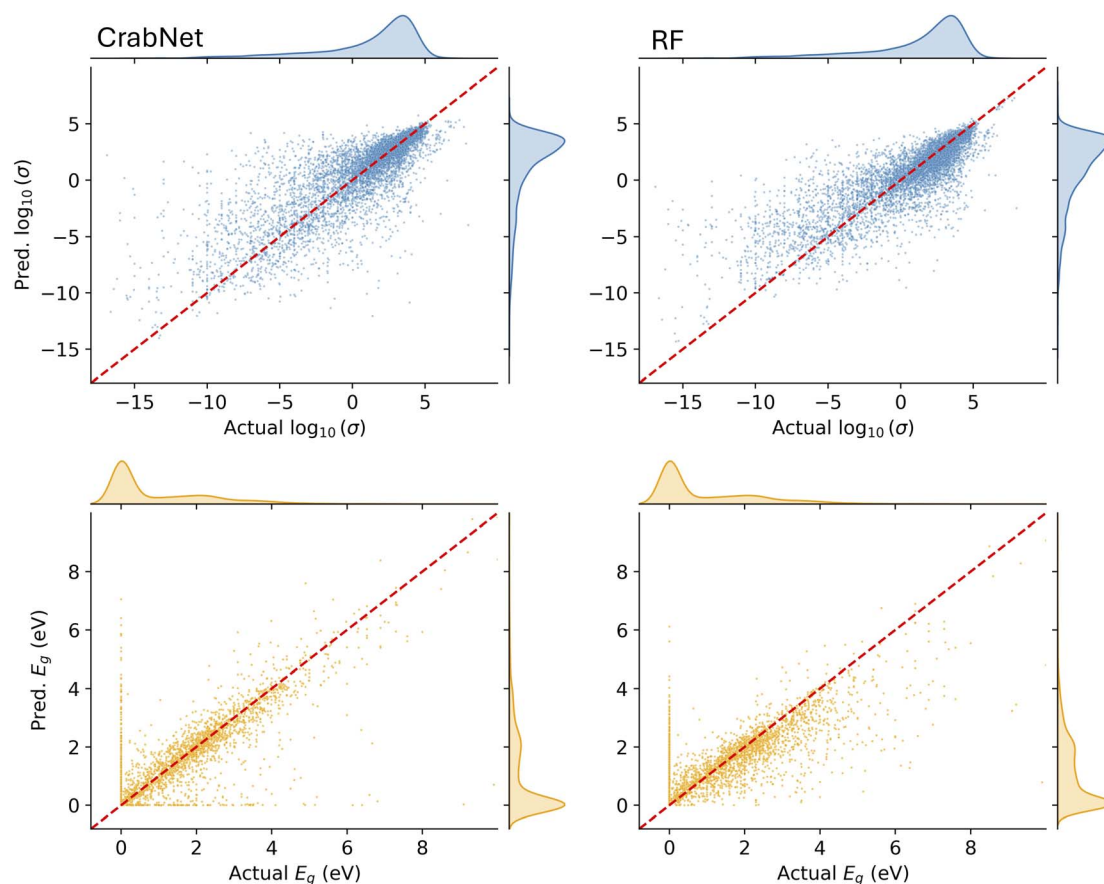


Fig. 4 Parity plots are shown for both electrical conductivity (top) and band gap (bottom) prediction. These were obtained by concatenating the different validation folds used in the K-fold evaluation scheme.

to a significant degradation in predictive performance, and contribute to an increased variance in the final evaluation. For example, *cluster 1* depicted in orange in Fig. 3 contains around 95% of the oxides in the entire dataset. This highlights

a scenario where the extrapolation task becomes too demanding for the model, as it is required to identify a great variability across multiple orders of magnitude, all without prior exposure to such conditions in the training dataset.



**5.1.2 Band gap prediction.** In the case of band gap, it is possible to observe a remarkable improvement of CrabNet compared to RF, with a decrease in MAE of  $\sim 27\%$ , and a slight average improvement in terms of  $R^2$ , although not statistically significant. In this scenario, we posit that the adoption of transfer learning provides a significant contribution (see Section 5.2). This trend is also partially evident in the LOCO-CV task; nevertheless, once again, the high variability poses challenges for a precise analysis in the out-of-distribution scenario. We believe that increasing the number of clusters can mitigate this issue, by ensuring a more consistent size of the training dataset in each iteration. However, a larger number of clusters increases the likelihood of similar data points being shared between the training and testing datasets, limiting the out-of-distribution assessment. Further exploration of this trade-off will be addressed in future research.

## 5.2 Identification of metals and non-metals

Accurate band gap prediction is critical for our ML pipeline. However, challenges arise due to the imbalance between metals and non-metals in material datasets, leading to frequent misclassification of metals as semiconductors or insulators, which can undermine prediction reliability.<sup>6</sup> Various strategies have been explored to mitigate this issue. A first attempt might be partitioning the task into two stages. The initial stage entails training a classifier to discriminate materials into metals and non-metals, eventually using loss-weighting schemes to limit the impact of class imbalances. The next stage would involve a regression task on the subset of non-metals by the preceding classification step. These methods have shown a limited effectiveness in practice.<sup>6</sup> We believe that an interesting alternative may involve foundation models pre-trained on large multi-domain datasets,<sup>77</sup> to be then fine-tuned for specific tasks with limited data.<sup>78</sup> However, we argue that a key concern with foundation models is potential data leakage during pre-training, which can lead to overly optimistic results in downstream tasks.

In our study, to enhance the accuracy of band gap identification, and thus minimizing the number of false negatives (in our definition, *metals* that are wrongly predicted as *semi-conductors* or *insulators*), we have utilized a transfer learning approach. This involved pre-training CrabNet on an extensive dataset sourced from the Materials Project,<sup>3</sup> encompassing all entries with chemical formulas and associated band gap information. At the time of data retrieval, 153 224 material entries with their corresponding band gaps were present in the Materials Project v2023.11.1 database. From this initial dataset, we filtered out chemical formulas that were deemed equivalent in our experimental band gap dataset, encompassing 4767 material entries. We have used the reduced chemical formula as criterion to establish equivalent entries, as atomic proportions are utilized when creating inputs to ML models. To ensure a fair evaluation we have discarded all such entries, ending up with a pretraining dataset consisting of 149 714 data points. Further processing is conducted on the resulting data to handle duplicates. We utilize a similar strategy akin to that employed for the experimental  $E_g$  dataset. Once duplicated material groups are identified, we eliminate those with a standard deviation exceeding 0.1 eV in terms of the corresponding band gaps. We have used this pool of data to pretrain CrabNet on DFT-calculated band gaps. This is later fine-tuned on our experimental  $E_g$  dataset.

In terms of regression metrics, the fine-tuned model demonstrates enhancements of roughly  $\approx 20\%$  in MAE and  $\approx 10\%$  in terms of  $R^2$ . To better evaluate the fine-tuned model's effectiveness in reducing false negatives, we investigate the predictions from both the original and fine-tuned models from a classification perspective. For a comprehensive assessment, we also include RF predictions within this evaluation. First, a simple rounding scheme is applied to all the obtained predictions. Specifically, predicted band gaps that are zero when rounded to two decimal places (*i.e.*, values less than 0.005) are assigned a label of 0, indicating metals. Predicted band gaps that round to non-zero values (*i.e.*, 0.005 or greater) are assigned a label of 1, indicating non-metals.

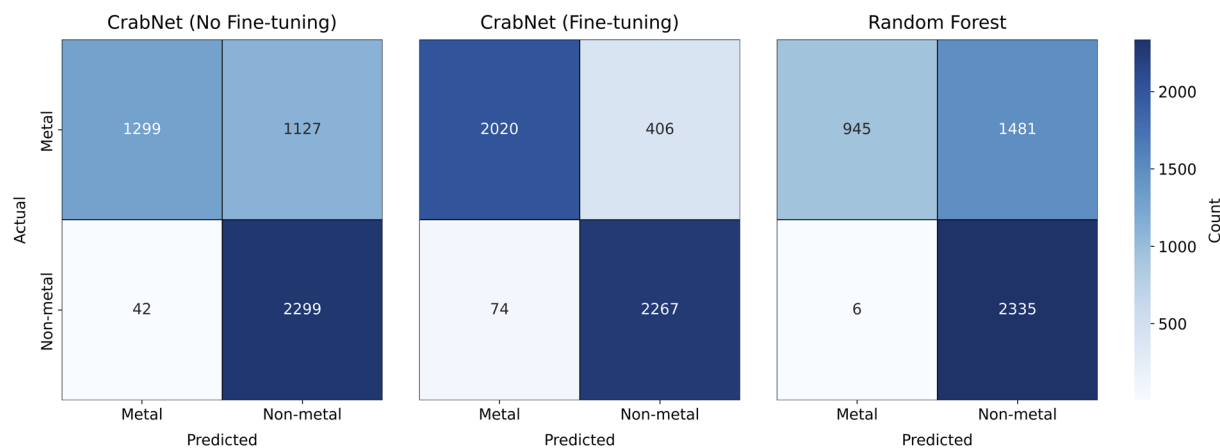


Fig. 5 Confusion matrices for the metal vs. non-metal classification task are displayed for the standard CrabNet (left), fine-tuned CrabNet (center), and RF. The fine-tuned CrabNet shows a remarkable improvement, with a significant reduction in false negatives compared to both the standard CrabNet and RF models.



In Fig. 5 we report the confusion matrices related to the different models considered. In terms of CrabNet, a significant decrease is observed in the count of false negatives, from the initial model (1127) to the fine-tuned one (406). This improvement comes with a slight increase in false positives (instances where semiconductors or insulators are incorrectly predicted as metals), rising from 42 in the model without fine-tuning to 74 in the fine-tuned model. For RF, we note a significant tendency to overestimate band gaps, resulting in a large number of metals being incorrectly predicted as non-metals (1481). Interestingly, in terms of false positives, only 6 non-metals are misclassified as metals. Further investigation on this aspect is deferred to future research. Additionally, we utilize *Matthews correlation coefficient* (MCC)<sup>79</sup> as a robust metric to quantify models' performance on binary classification, given its suitability for imbalanced data. It is defined as follows:

$$\text{MCC} := \frac{(\text{TP} \times \text{TN}) - (\text{FP} \times \text{FN})}{\sqrt{(\text{TP} + \text{FP})(\text{TP} + \text{FN})(\text{TN} + \text{FP})(\text{TN} + \text{FN})}}, \quad (5)$$

with TP, TN, FP, FN denoting, as usual, *true positives*, *true negatives*, *false positives*, and *false negatives*, respectively. A significant improvement is observed when comparing CrabNet

without fine-tuning to the fine-tuned version, with the MCC increasing from 0.58 to 0.80. Conversely, the MCC obtained from the RF model is 0.48, which is significantly lower. This can be attributed to the tendency of the model in overestimating the band gaps, leading to a high number of false negatives. Considering the pivotal role that band gap prediction plays in the primary objective of this work, namely accelerating the identification of new TCMs, we believe that this analysis holds fundamental significance. In this context, improving the precision of ML models in discriminating metals from non-metals greatly facilitates the selection of promising material subsets for further investigation.

### 5.3 Leave-one-TCM-family-out

We have discussed the results of two classic evaluation schemes, which carry intrinsic limitations. On the one hand, K-fold provides limited insights on the real possibilities of identifying materials outside the training distribution, frequently yielding overestimated results. On the other hand, LOCO-CV often leads to a noisy evaluation, due to the different size of the obtained material clusters. In Fig. 6, we present the results obtained from the proposed leave-one-TCM-family-out

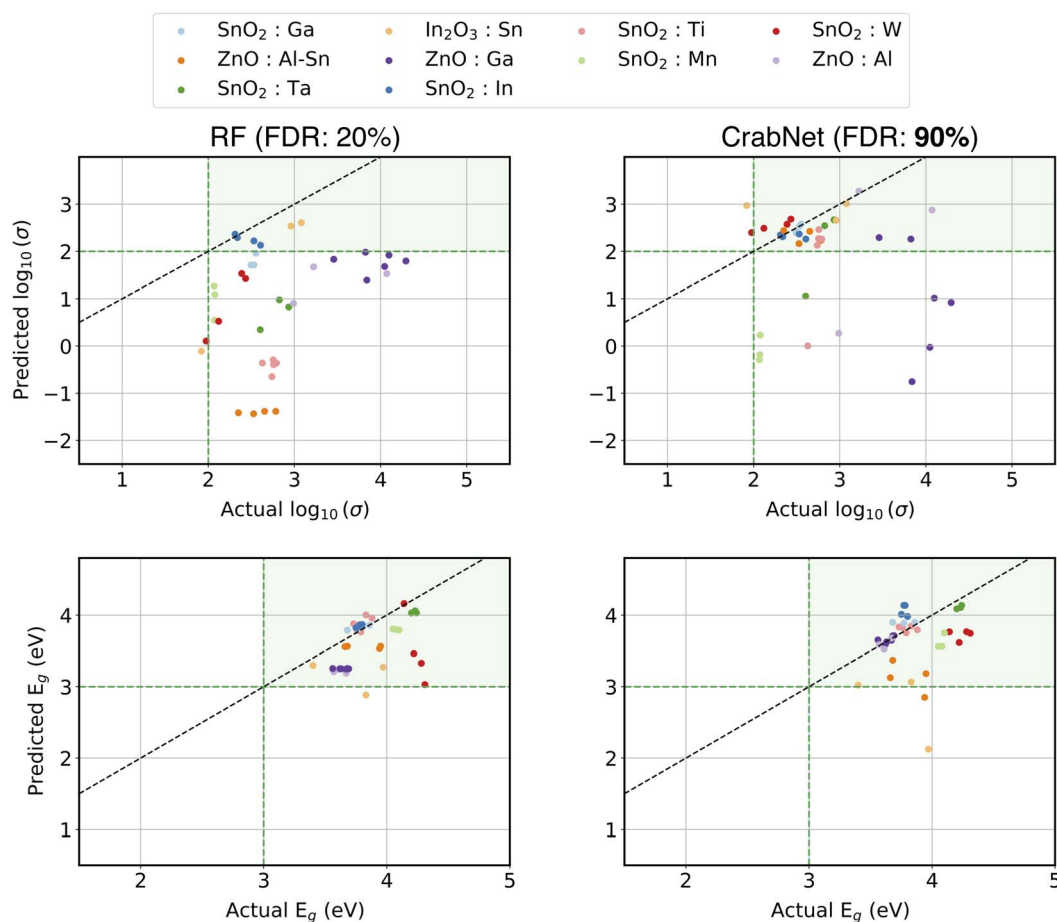


Fig. 6 Predicted test TCMs within the leave-one-TCM-family-out evaluation setting, categorized by the constituent properties of electrical conductivity (top) and band gap (bottom). The FDR score indicates the percentage of test TCM families correctly identified by the models, *i.e.* test materials correctly predicted with respect to the thresholds of  $10^2 \text{ S cm}^{-1}$  for conductivity, and 3 eV for band gap.



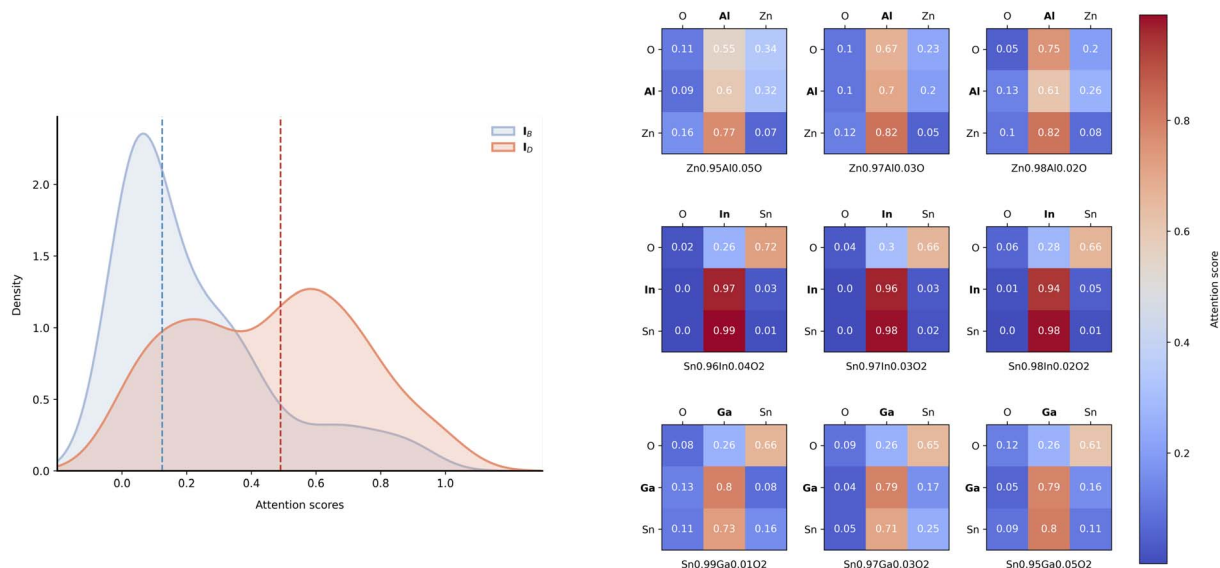


Fig. 7 Distributions of attention scores categorized in terms of interaction with base elements  $I_B$  and with dopants  $I_D$  (left). Examples of attention matrices extracted for test TCMs in the leave-one-TCM-family out evaluation scheme (right), with dopant elements highlighted in bold.

benchmark, showcasing the joint predictions of both RF and CrabNet and for both properties under consideration ( $\sigma$  and  $E_g$ ). We notice that CrabNet is the only model capable of identifying the majority of TCMs families in the test set, achieving an FDR of 90%, compared to 20% obtained by RF. The main challenge results in the identification of electrical conductivity in these materials. As shown in Fig. 6, RF significantly underestimates this property. However, in the case of band gap prediction, both models correctly identify over 90% of the total materials. We believe this is primarily due to the smoother relationship between stoichiometry and band gap, which simplifies the out-of-distribution evaluation. Overall, our analysis shows a superior robustness of CrabNet in identifying novel stoichiometric combinations that were not present in the training distribution.

#### 5.4 Predictions explainability via attention scores

Although the significant breakthroughs enabled by deep learning in materials informatics, the *interpretability* of these methods still remains severely limited, giving rise to entire branches of research which aim to improve human understanding of ML models (*explainable AI*).<sup>80</sup> The interpretability of ML is indeed a crucial aspect, that acquires further importance in scientific applications, often characterized by collaboration among researchers from various fields, and with different backgrounds. However, current approaches often rely on black-box functions, which offer limited insights into the decision-making process. Notably, the transformer architecture<sup>63</sup> provides an inherent mechanism for interpreting its decision-making process through the use of self-attention. The analysis of the underlying attention scores can indeed offer insights about tokens' significance with respect to the surrounding context.

To investigate the superior predictive accuracy achieved by CrabNet in conductivity prediction, we examined the

corresponding attention scores generated during the leave-one-TCM-family-out evaluation scheme. Specifically, we extracted attention scores from the last layer of the CrabNet encoder, averaged by the corresponding number of attention heads. In this context, we aim to understand whether the model captures complex chemical phenomena related to doping. In this context, we indicate with  $B = \{b_1, \dots, b_n\}$  the *base* elements, *i.e.* those which are present in the pristine form of the material, while with  $D = \{d_1, \dots, d_k\}$  we indicate the *dopant* elements in the chemical formula. For example, for Zn<sub>0.95</sub>Al<sub>0.05</sub>O we have  $B = \{Zn, O\}$  and  $D = \{Al\}$  while for Zn<sub>0.97</sub>Al<sub>0.02</sub>Sn<sub>0.01</sub>O<sub>2</sub> we have  $B = \{Zn, O\}$  and  $D = \{Al, Sn\}$ . We categorize entries of the attention matrices into four interaction groups:

- $A_{BB} = [A_{ij}]$  with  $e_i, e_j \in B$  for *base–base* interactions;
- $A_{BD} = [A_{ij}]$  with  $e_i \in B, d_j \in D$  for *base–dopant* interactions;
- $A_{DD} = [A_{ij}]$  with  $d_i, d_j \in D$  for *dopant–dopant* interactions;
- $A_{DB} = [A_{ij}]$  with  $d_i \in D, e_j \in B$  for *dopant–base* interactions.

The interactions involving base elements,  $I_B = A_{DB} \cup A_{BB}$ , and those involving dopants,  $I_D = A_{BD} \cup A_{DD}$ , reveal distinct patterns in the attention scores. As shown in Fig. 7 (left), the distribution of  $I_D$  exhibits a clear shift towards higher attention scores compared to  $I_B$ , with the medians indicated by dotted lines. This suggests that the model assigns a greater importance to the interactions involving dopants, effectively capturing their critical role in shaping material representations for conductivity prediction.

## 6 Testing the search for new TCMs

To assess ML models' effectiveness in identifying TCMs, a search was conducted in the Pearson's Crystallographic Database,<sup>16</sup> MPDS<sup>4</sup> and ICSD<sup>17</sup> (based on available data as of December 2024) for compounds containing elements commonly found in known classes of TCMs. Predicting their



properties with ML could reveal materials previously overlooked as TCMs. For this experiment, we utilize CrabNet, given its good performance in the proposed leave-one-TCM-family-out evaluation method.

We conducted a search for oxide compounds containing combinations of three cations from Zn, Ga, Sn, Al, and In. We also include a small selection of five compositions across MPDS and ICSD of doped binary oxides (ZnO, SnO<sub>2</sub> and In<sub>2</sub>O<sub>3</sub>), with

dopants not present in the training dataset. We end up with a final list comprising 55 compositions shown in Table 4.

We utilize the same TCMs criteria established for the leave-one-TCM-family-out evaluation. Specifically, we are targeting materials with band gap  $E_g > 3$  eV and with conductivity  $\sigma > 10^2$  S cm<sup>-1</sup>. Compositions meeting these criteria are highlighted in Table 4. To provide a global assessment of ML-predicted materials, we define a figure of merit  $\Phi_M$  as:

**Table 4** Predicted values of conductivity ( $\sigma$ ) and band gap ( $E_g$ ) for a set of materials containing elements common to known classes of TCMs *i.e.* oxides with combinations of Zn, Al, Ga, In and Sn, with additional dopant elements.  $\Phi_M$ ,  $\Phi_M^{\text{std}}$  and  $\Phi_M^{\text{std-adj}}$  are figure of merit values as discussed in the main text. Databases in which the compositions were searched are given in the *Source* column. Red-bordered cells indicate materials meeting our TCMs criteria, with a conductivity greater than  $2(\log_{10}(\text{S cm}^{-1}))$ , and a band gap greater than 3 eV. Rows with formula high-lighted in blue are doped binary oxides of Zn, Sn or In, closest to the training dataset; unhighlighted rows are three cation oxide materials with constituent elements commonly found within well-known TCM classes. Compositions are ordered from highest to lowest  $\Phi_M^{\text{std-adj}}$  (ref. 81–100)

| #  | Source  | Formula  | $\sigma_{\text{pred}} (\log_{10}(\text{S cm}^{-1}))$ | $E_{g,\text{pred}} (\text{eV})$ | $\Phi_M$ | $\Phi_M^{\text{std}}$ | $\Phi_M^{\text{std-adj}}$ | $\sigma_{\text{exp}} (\log_{10}(\text{S cm}^{-1}))$ | $E_{g,\text{exp}} (\text{eV})$ | Ref.      |
|----|---------|--|--|---------------------------------|----------|-----------------------|---------------------------|---|--------------------------------|-----------|
| 1  | PEARSON | Al <sub>0.67</sub> Ga <sub>1.33</sub> Zn <sub>37</sub> O <sub>40</sub>     | 3.42   | 3.57                            | 12.20    | 1.90                  | 10.29                     | 2.30-3.00   | —                              | 81        |
| 2  | MPDS    | Na <sub>0.025</sub> Zn <sub>0.975</sub> O <sub>1.988</sub>                 | 3.14   | 3.74                            | 11.75    | 3.73                  | 8.02                      | —   | 3.26                           | 82        |
| 3  | MPDS    | Ca <sub>0.04</sub> Zn <sub>0.96</sub> O                                    | 3.12   | 4.02                            | 12.53    | 4.69                  | 7.84                      | 1.30  | 3.40                           | 83        |
| 4  | MPDS    | Sn <sub>0.98</sub> Ge <sub>0.02</sub> O <sub>2</sub>                       | 2.40   | 4.19                            | 10.07    | 2.58                  | 7.49                      | —   | —                              | —         |
| 5  | ICSD    | Cr <sub>0.02</sub> Sn <sub>0.98</sub> O <sub>1.99</sub>                    | 2.53   | 3.73                            | 9.41     | 1.94                  | 7.47                      | —   | —                              | —         |
| 6  | PEARSON | Ga <sub>0.06</sub> In <sub>1.92</sub> Sn <sub>0.02</sub> O <sub>3.01</sub> | 2.92   | 3.52                            | 10.29    | 3.71                  | 6.58                      | 3.48  | 3.10                           | 84        |
| 7  | PEARSON | AlInZn <sub>21</sub> O <sub>24</sub>                                       | 2.81   | 3.31                            | 9.31     | 2.91                  | 6.40                      | —   | —                              | —         |
| 8  | PEARSON | In <sub>1.68</sub> Sn <sub>0.16</sub> Zn <sub>0.16</sub> O <sub>3</sub>    | 3.08   | 2.86                            | 8.80     | 2.57                  | 6.23                      | 2.81  | 2.59                           | 85        |
| 9  | PEARSON | Ga <sub>1.5</sub> In <sub>0.5</sub> Zn <sub>11</sub> O <sub>14</sub>       | 2.79   | 3.12                            | 8.71     | 2.65                  | 6.06                      | —   | —                              | —         |
| 10 | PEARSON | GaInZn <sub>6</sub> O <sub>9</sub>   | 2.45   | 3.01                            | 7.40     | 2.91                  | 4.49                      | 2.60  | 3.10                           | 86 and 87 |
| 11 | PEARSON | AlInZn <sub>11</sub> O <sub>14</sub>                                       | 2.37   | 3.04                            | 7.21     | 2.96                  | 4.25                      | —   | —                              | —         |
| 12 | PEARSON | GaSn <sub>0.5</sub> Zn <sub>6.5</sub> O <sub>9</sub>                       | 2.32   | 3.06                            | 7.10     | 2.87                  | 4.22                      | —   | —                              | —         |
| 13 | PEARSON | GaInZn <sub>11</sub> O <sub>14</sub>                                       | 2.40   | 3.06                            | 7.36     | 3.64                  | 3.72                      | —   | —                              | —         |
| 14 | PEARSON | Al <sub>0.4</sub> In <sub>1.6</sub> Zn <sub>3</sub> O <sub>8</sub>         | 2.25   | 3.34                            | 7.51     | 3.84                  | 3.67                      | —   | —                              | —         |
| 15 | PEARSON | GaInZn <sub>7</sub> O <sub>10</sub>  | 2.36   | 2.90                            | 6.84     | 3.27                  | 3.57                      | 1.46  | 3.05                           | 88 and 89 |
| 16 | PEARSON | AlInZn <sub>9</sub> O <sub>12</sub>  | 2.19   | 3.11                            | 6.81     | 3.29                  | 3.52                      | —   | —                              | —         |
| 17 | PEARSON | Al <sub>0.75</sub> In <sub>1.25</sub> Zn <sub>6</sub> O <sub>9</sub>       | 2.05   | 3.35                            | 6.86     | 3.51                  | 3.35                      | —   | —                              | —         |
| 18 | PEARSON | GaInZn <sub>13</sub> O <sub>16</sub>                                       | 2.38   | 3.04                            | 7.23     | 4.29                  | 2.94                      | —   | —                              | —         |
| 19 | PEARSON | GaInZn <sub>9</sub> O <sub>12</sub>  | 2.23   | 3.15                            | 7.01     | 4.20                  | 2.81                      | —   | 3.02                           | 89        |
| 20 | PEARSON | GaInZn <sub>3</sub> O <sub>8</sub>   | 2.28   | 3.36                            | 7.67     | 4.93                  | 2.74                      | -3.30   | 3.12                           | 90 and 89 |
| 21 | PEARSON | GaSn <sub>0.5</sub> Zn <sub>7.5</sub> O <sub>10</sub>                      | 2.11   | 3.04                            | 6.44     | 3.78                  | 2.66                      | —   | —                              | —         |
| 22 | PEARSON | Al <sub>0.75</sub> In <sub>1.25</sub> Zn <sub>3</sub> O <sub>8</sub>       | 2.17   | 3.17                            | 6.90     | 4.56                  | 2.34                      | —   | —                              | —         |
| 23 | PEARSON | AlInZn <sub>7</sub> O <sub>10</sub>  | 2.34   | 2.63                            | 6.16     | 3.88                  | 2.28                      | —   | —                              | —         |
| 24 | PEARSON | AlInZn <sub>13</sub> O <sub>16</sub>                                       | 2.31   | 2.77                            | 6.40     | 4.44                  | 1.96                      | —   | —                              | —         |
| 25 | MPDS    | Hf <sub>0.03</sub> In <sub>1.97</sub> O <sub>3</sub>                       | 2.44   | 3.94                            | 9.61     | 7.73                  | 1.88                      | —   | —                              | —         |
| 26 | PEARSON | AlInZn <sub>15</sub> O <sub>18</sub>                                       | 1.98   | 3.08                            | 6.10     | 4.77                  | 1.32                      | —   | —                              | —         |
| 27 | PEARSON | AlInZn <sub>19</sub> O <sub>22</sub>                                       | 1.95   | 3.23                            | 6.31     | 5.24                  | 1.07                      | —   | —                              | —         |
| 28 | PEARSON | Al <sub>0.75</sub> In <sub>1.25</sub> Zn <sub>4</sub> O <sub>7</sub>       | 1.71   | 2.70                            | 4.61     | 4.76                  | -0.15                     | —   | —                              | —         |
| 29 | PEARSON | Al <sub>0.75</sub> In <sub>1.25</sub> Zn <sub>5</sub> O <sub>10</sub>      | 2.17   | 2.06                            | 4.46     | 4.66                  | -0.19                     | —   | —                              | —         |
| 30 | PEARSON | AlInZn <sub>7</sub> O <sub>10</sub>  | 1.69   | 3.27                            | 5.51     | 5.82                  | -0.31                     | —   | —                              | —         |
| 31 | PEARSON | AlInZn <sub>5</sub> O <sub>8</sub>   | 1.81   | 3.08                            | 5.56     | 6.54                  | -0.98                     | —   | —                              | —         |
| 32 | PEARSON | Al <sub>0.04</sub> Sn <sub>0.98</sub> Zn <sub>1.98</sub> O <sub>4</sub>    | 0.73   | 2.34                            | 1.72     | 3.75                  | -2.03                     | 0.89  | 3.50                           | 91        |
| 33 | PEARSON | GaInZn <sub>4</sub> O <sub>7</sub>   | 0.64   | 3.18                            | 2.05     | 8.96                  | -6.92                     | 2.61  | 2.85                           | 92        |
| 34 | PEARSON | AlInZn <sub>4</sub> O <sub>7</sub>   | 0.36   | 3.23                            | 1.16     | 8.28                  | -7.12                     | —   | —                              | —         |
| 35 | PEARSON | Al <sub>0.5</sub> In <sub>1.5</sub> Zn <sub>2</sub> O <sub>5</sub>         | -0.65  | 3.35                            | -2.19    | 7.15                  | -9.34                     | —   | —                              | —         |
| 36 | PEARSON | Al <sub>0.75</sub> In <sub>1.25</sub> Zn <sub>3</sub> O <sub>6</sub>       | -0.08  | 3.43                            | -0.27    | 9.73                  | -10.00                    | —   | —                              | —         |
| 37 | PEARSON | In <sub>0.8</sub> Sn <sub>0.6</sub> Zn <sub>0.6</sub> O <sub>3</sub>       | -0.91  | 2.97                            | -2.71    | 9.06                  | -11.76                    | —   | —                              | —         |
| 38 | PEARSON | AlInZn <sub>3</sub> O <sub>6</sub>   | -0.70  | 3.62                            | -2.52    | 13.19                 | -15.71                    | —   | —                              | —         |
| 39 | PEARSON | GaInZn <sub>3</sub> O <sub>6</sub>   | -0.54  | 3.36                            | -1.80    | 14.00                 | -15.80                    | 2.23  | 2.95                           | 92        |
| 40 | PEARSON | AlInZn <sub>3</sub> O <sub>5</sub>   | -1.57  | 3.71                            | -5.81    | 12.88                 | -18.70                    | —   | —                              | —         |
| 41 | PEARSON | GaInZn <sub>3</sub> O <sub>5</sub>   | -2.34  | 3.29                            | -7.70    | 12.04                 | -19.75                    | 2.45  | 2.95/ 3.16                     | 92 and 93 |
| 42 | PEARSON | Ga <sub>2</sub> In <sub>6</sub> Sn <sub>2</sub> O <sub>16</sub>            | -1.92  | 3.49                            | -6.72    | 14.49                 | -21.21                    | 1.26  | 2.67                           | 94        |
| 43 | PEARSON | Ga <sub>1.9</sub> In <sub>0.1</sub> Zn <sub>4</sub> O <sub>4</sub>         | -3.34  | 3.69                            | -12.32   | 12.32                 | -24.64                    | —   | 4.18                           | 95        |
| 44 | PEARSON | Ga <sub>2.8</sub> In <sub>1.2</sub> Sn <sub>2</sub> O <sub>12</sub>        | -4.88  | 3.48                            | -16.97   | 10.69                 | -27.66                    | —   | —                              | —         |
| 45 | PEARSON | Ga <sub>3</sub> InSn <sub>3</sub> O <sub>12</sub>                          | -5.26  | 3.49                            | -18.40   | 12.51                 | -30.91                    | —   | —                              | —         |
| 46 | PEARSON | Ga <sub>1.4</sub> In <sub>0.6</sub> Sn <sub>3</sub> O <sub>5</sub>         | -5.05  | 3.51                            | -17.71   | 13.23                 | -30.95                    | —   | —                              | —         |
| 47 | PEARSON | Ga <sub>2.8</sub> In <sub>1.2</sub> Sn <sub>2</sub> O <sub>16</sub>        | -5.01  | 3.54                            | -17.74   | 13.34                 | -31.07                    | —   | —                              | —         |
| 48 | PEARSON | Ga <sub>2</sub> In <sub>2</sub> ZnO <sub>7</sub>                           | -4.86  | 3.64                            | -17.69   | 14.34                 | -32.03                    | -1.00   | 3.00                           | 96        |
| 49 | PEARSON | Ga <sub>3</sub> InSn <sub>3</sub> O <sub>16</sub>                          | -4.92  | 3.58                            | -17.62   | 14.79                 | -32.41                    | -5.00   | 3.58                           | 97        |
| 50 | PEARSON | Ga <sub>1.55</sub> In <sub>0.45</sub> Sn <sub>0.5</sub> O <sub>5</sub>     | -4.65  | 3.73                            | -17.32   | 15.93                 | -33.25                    | —   | —                              | —         |
| 51 | PEARSON | Al <sub>0.52</sub> Ga <sub>1.48</sub> ZnO <sub>4</sub>                     | -5.62  | 3.34                            | -18.74   | 17.14                 | -35.88                    | —   | 4.60                           | 98        |
| 52 | PEARSON | Al <sub>1.52</sub> Ga <sub>0.48</sub> ZnO <sub>4</sub>                     | -5.28  | 3.78                            | -19.98   | 20.12                 | -40.10                    | —   | 5.20                           | 98        |
| 53 | PEARSON | AlInZnO <sub>4</sub>   | -6.23  | 3.69                            | -22.99   | 17.78                 | -40.77                    | —   | —                              | —         |
| 54 | PEARSON | GaInZnO <sub>4</sub>   | -6.53  | 3.26                            | -21.27   | 19.80                 | -41.07                    | 2.41  | 3.00                           | 92 and 99 |
| 55 | PEARSON | AlGaZnO <sub>4</sub>   | -9.12  | 2.34                            | -21.35   | 32.84                 | -54.20                    | —   | 4.65                           | 100       |



$$\Phi_M = \hat{E}_g \times \hat{\sigma}, \quad (6)$$

where  $\hat{E}_g$  and  $\hat{\sigma}$  denote the predicted band gap and conductivity (as  $\log_{10}$ ) from ML models' ensembles, respectively. In essence,  $\Phi_M$  will prioritize an optimal trade-off between the two properties. We further utilize a risk-adjusted figure of merit  $\Phi_M^{\text{std-adj}}$ ,<sup>6</sup> defined as

$$\Phi_M^{\text{std-adj}} = \Phi_M - \Phi_M^{\text{std}}, \quad (7)$$

where  $\Phi_M^{\text{std}} = \sqrt{\hat{E}_g^2 s_{\hat{E}_g}^2 + \hat{\sigma}^2 s_{\hat{\sigma}}^2}$  is obtained by uncertainty propagation rules for multiplication, and  $s_P$  denotes the uncertainty produced by an ensemble of ML models (standard deviation corresponding to the predictive mean, see ESI†) for a predicted property  $P$ . The risk-adjusted figure of merit  $\Phi_M^{\text{std-adj}}$  is essentially defined by subtracting one standard deviation from the original figure of merit  $\Phi_M$ . Compositions with high figure of merit and low uncertainty in their prediction are prioritised over compositions with large uncertainty in their prediction.

From the analysis of the model outputs of the 55 materials selected above, the compositions with the highest  $\Phi_M^{\text{std-adj}}$  are, as expected, those most similar to the training dataset; we discuss the results for a selection of the other compositions here. Doped binary oxides are ranked high by  $\Phi_M$  and their band gaps are accurately predicted.  $\text{Na}_{0.025}\text{Zn}_{0.975}\text{O}_{0.988}$  (entry 2) is predicted to have a conductivity of 3.14 ( $\log_{10}(\text{S cm}^{-1})$ ), although measurements reported in the literature are much lower, due to the low concentration of p-type carriers.<sup>82</sup> The band gap prediction of  $\text{Na}_{0.025}\text{Zn}_{0.975}\text{O}_{0.988}$  (3.74 eV), compares to the reported experimental measurement of 3.26 eV.<sup>101</sup> Thin films of  $\text{Ca}_{0.04}\text{Zn}_{0.96}\text{O}$  (entry 3) exhibit a band gap of 3.40 eV and a conductivity of 1.3 ( $\log_{10}(\text{S cm}^{-1})$ ),<sup>83</sup> though the nature of the conductivity is not discussed in the report and  $\text{Ca}^{2+}$  doped ZnO would not be expected to display electrical conductivity. CrabNet predicts a band gap of 4.02 eV and a conductivity of 3.12 ( $\log_{10}(\text{S cm}^{-1})$ ) for this composition. Both the band gap and conductivity predictions show consistency with the expected error ranges outlined in Tables 2 and 3. The higher deviation in conductivity predictability is considered acceptable given the inherent complexity of predicting conductivity solely from stoichiometry. Notably, neither {Ca, Zn, O} nor {Na, Zn, O} phase fields are present in the training dataset. For materials containing three cations, indium-containing phase fields rank near the top (Table 4). This is expected, given the well-established significance of  $\text{In}_2\text{O}_3$  in the TCMs literature. Materials in the  $\text{Ga}_2\text{O}_3\text{-In}_2\text{O}_3\text{-SnO}_2$  phase field<sup>102</sup> have been explored as transparent conductors,<sup>99</sup> with the highest-ranking material in the phase field  $\text{Ga}_{0.06}\text{In}_{1.92}\text{Sn}_{0.02}\text{O}_{3.01}$  (entry 6) having a reported conductivity of 3.43 ( $\log_{10}(\text{S cm}^{-1})$ ) and a band gap of 3.04 eV (ref. 84) which the model does well at predicting with 2.92 ( $\log_{10}(\text{S cm}^{-1})$ ) for conductivity and 3.52 eV for band gap. The highest  $\Phi_M^{\text{std-adj}}$ -ranked material,  $\text{Al}_{0.67}\text{Ga}_{1.33}\text{Zn}_{37}\text{O}_{40}$  (entry 1) is a homologous phase (( $\text{Ga}_{1-\alpha}\text{Al}_{\alpha}$ )<sub>2</sub> $\text{O}_3(\text{ZnO})_m$ ) in the pseudo-ternary  $\text{Ga}_2\text{O}_3\text{-Al}_2\text{O}_3\text{-ZnO}$  phase field and has been postulated as a potential thermoelectric<sup>81</sup> but not as a TCM, and

its band gap and electrical conductivity were not reported. Given that other materials in the  $\text{Ga}_2\text{O}_3\text{-Al}_2\text{O}_3\text{-ZnO}$  phase field have very high conductivity ( $1.0 \times 10^4$  to  $1.6 \times 10^4 \text{ S cm}^{-1}$ )<sup>81</sup> it could be expected that the composition  $\text{Al}_{0.67}\text{Ga}_{1.33}\text{Zn}_{37}\text{O}_{40}$  could also show high conductivity and an appropriate band gap. The Al doped  $\text{Zn}_2\text{SnO}_4$  spinel,  $\text{Al}_{0.04}\text{Sn}_{0.98}\text{Zn}_{1.98}\text{O}_4$  (entry 32 in Table 4) has been explored as TCM for CIGS solar cells,<sup>91</sup> and has a measured band gap of >3.5 eV but low conductivity ( $12.9(\log_{10}(\text{S cm}^{-1}))$ ). Other spinel materials have had their conductivity measured, for example  $\text{GaInZnO}_4$  (entry 54) has a measured conductivity of 2.7 ( $\log_{10}(\text{S cm}^{-1})$ ) which is much higher than predicted ( $-6.53(\log_{10}(\text{S cm}^{-1}))$ ), and a band gap of 3.5 eV (ref. 103) which is predicted very closely (3.26 eV). These two examples show that the model recognizes that doping small amounts of elements into structures can induce conductivity ( $\text{Al}_{0.04}\text{Sn}_{0.98}\text{Zn}_{1.98}\text{O}_4$ ) and more stoichiometric closed shell materials are less likely to display conductivity ( $\text{GaInZnO}_4$ ). In fact, the measured conductivity in  $\text{GaInZnO}_4$  results from Ga anti-site defects,  $\text{Ga}_{\text{Zn}}$ , as the major electron donor in  $\text{GaInZnO}_4$  (ref. 104) which would be difficult for an ML model to capture, when trained on composition only. This is because the oxidation states present would correspond to filled bands and thus to a low conductivity in terms of electron count, while the model is unable to recognise the self-doping that produces the experimentally observed conductivity.

## 7 Limitations

While we believe our analysis has provided valuable insights into leveraging data-driven methods for accelerating the discovery of new TCMs, it is important to acknowledge certain limitations inherent in our approach. As with all ML models, they should be used and the outputs assessed by a domain expert for the full benefits to be realised.

The first challenge stems from the inherently limited pool of existing TCMs. Given the scarcity of such materials in current databases or literature, our data-driven pipeline is inevitably constrained, impacting the breadth and depth of the proposed analysis.

A second limitation relates to the specific mechanisms underlying the properties of the materials of interest. If the goal is to identify TCMs similar to those in the training dataset, the proposed framework is indeed promising, as shown in Table 4. However, when seeking materials that achieve the desired properties through different mechanisms, our approach is less likely to provide new insights into the underlying chemistry. For example, the model reported here will not distinguish between n-type and p-type conductivity, as highlighted in Section 6, and the outputs will need to be interpreted by the expert user. This is because data-driven frameworks largely depends on the patterns reflected in the training dataset, which may not capture the diversity of mechanisms outside the established categories. This limitation was already highlighted in previous work.<sup>9,105</sup>

Another limitation arises from the nature of the input data used in this study, which focuses solely on the stoichiometry of materials. In exploratory settings, stoichiometry-based methods



provide a valuable and natural baseline since structural information is typically unavailable. However, when additional information is available, it becomes essential to incorporate it effectively. Moving forward, we foresee the integration of more detailed prior knowledge as an important next step. This could involve leveraging recent developments in Large Language Models (LLMs) to encode domain knowledge in chemistry, as suggested by ref. 106 and 78, or incorporating structural data *via* representation learning schemes.<sup>67,107</sup>

## 8 Conclusions

We have proposed a bespoke data-driven framework aimed at leveraging data-driven methods to accelerate the discovery of new TCMs. To address the challenge of limited and sparse material data, we created two experimental datasets of room-temperature conductivity and band gap. This involved the collection of raw data, followed by the application of a meticulous, line-by-line validation to verify the correctness of the reported chemical formulas, alongside the corresponding measurements of electrical conductivity and band gap. The validated datasets were used as foundation for evaluating SOTA ML models for property-prediction from the stoichiometry alone. We have proposed a bespoke evaluation method to empirically measure the potential of ML in identifying new classes of TCMs. Finally, we have compiled a list of 55 compositions sourced across various material databases, to test the effectiveness of ML in accelerate the identification of new TCMs. Overall, our results suggest that ML has the potential to identify new TCMs that are compositionally similar to the ones in the training dataset. Nonetheless, we argue that this holds significant value, as it enables an accelerated identification of compounds that may have been previously overlooked as TCMs.

## 9 Implementation details

CrabNet has been implemented with a batch size of 512, a RobustL1 loss function, a Lamb Lookahead optimizer with stochastic weight averaging, a cyclic learning rate from  $1 \times 10^{-4}$  to  $6 \times 10^{-3}$ . For RF, we used a modified scikit-learn implementation to estimate aleatoric and epistemic contributions to uncertainties.<sup>60</sup> This involved fitting two RF models: one for point predictions and epistemic uncertainty, quantified as the standard deviation across predictions within trees in the ensemble ( $n\_estimators = 500$ ,  $min\_samples\_split = 2$ ,  $min\_samples\_leaf = 1$ ), and another for aleatoric uncertainty, which was identical except for  $min\_samples\_leaf = 10$ , as suggested in ref. 60.

## Code availability

The code supporting the main results of this study is available on GitHub at <https://github.com/fedeotto/tcms>. Code repository has been archived on Zenodo at <https://doi.org/10.5281/zenodo.15366904>. Instructions for obtaining representative datasets to run the pipeline are included in the repository.

## Data availability

The electrical conductivity dataset used in this work was compiled from two primary sources: the UCSB Thermoelectric Database and the Materials Platform for Data Science (MPDS). The original UCSB dataset, consisting of approximately 1100 entries, was expanded as part of ongoing work by the original authors. This updated version, which was used in our study, is available at <https://zenodo.org/records/15365345> (DOI: [10.5281/zenodo.15365345](https://doi.org/10.5281/zenodo.15365345)). Due to licensing restrictions associated with MPDS data and confidentiality agreements tied to funding, we are unable to publicly release the full experimental conductivity dataset used in this study. Access to raw MPDS data requires a commercial API license, which can be obtained from <https://mpds.io/>.

The original, unmodified band gap dataset, used as the basis for the enriched version proposed in this study, is available through the original publication <https://pubs.acs.org/doi/10.1021/acs.jpcclett.8b00124> (DOI: [10.1021/acs.jpcclett.8b00124](https://doi.org/10.1021/acs.jpcclett.8b00124)). Due to confidentiality agreements tied to funding, we are unable to publicly release the modified band gap dataset used in this study.

Additional band gap data used for pre-training CrabNet were obtained from the Materials Project (version 2023.11.1), accessible *via* their API at <https://materialsproject.org>. Data from Pearson's Crystallographic Database are available through institutional or commercial subscription. Access to the Inorganic Crystal Structure Database (ICSD) similarly requires a commercial API license, available at <https://www.fiz-karlsruhe.de/icsd.html>.

## Conflicts of interest

There are no conflicts to declare.

## Acknowledgements

We thank EPSRC for support under EP/V026887/1 and the Impact Acceleration Account, Pilkington (NSG Group) and Leverhulme Trust through the Leverhulme Research Centre for Functional Materials Design (RC-2015-036).

## References

- G. R. Schleder, A. C. M. Padilha, C. M. Acosta, M. Costa and A. Fazzio, From DFT to machine learning: recent approaches to materials science—a review, *J. Phys.: Mater.*, 2019, **2**(3), 032001.
- R. Pollice, G. dos Passos Gomes, M. Aldeghi, R. J. Hickman, M. Krenn, C. Lavigne, *et al.*, Data-Driven Strategies for Accelerated Materials Design, *Acc. Chem. Res.*, 2021, **54**(4), 849–860.
- A. Jain, S. P. Ong, G. Hautier, W. Chen, W. D. Richards, S. Dacek, *et al.*, The Materials Project: A materials genome approach to accelerating materials innovation, *APL Mater.*, 2013, **1**(1), 011002.



- 4 E. Blokhin and P. Villars, The PAULING FILE Project and Materials Platform for Data Science: From Big Data Toward Materials Genome, *Handbook of Materials Modeling: Methods: Theory and Modeling*, 2018, pp. 1–26.
- 5 S. Kirklin, J. E. Saal, B. Meredig, A. Thompson, J. W. Doak, M. Aykol, *et al.*, The Open Quantum Materials Database (OQMD): assessing the accuracy of DFT formation energies, *npj Comput. Mater.*, 2015, **1**(1), 15010.
- 6 J. Riebesell, T. W. Surta, R. E. A. Goodall, M. W. Gaultois and A. A. Lee, Discovery of high-performance dielectric materials with machine-learning-guided search, *Cell Rep. Phys. Sci.*, 2024, **5**(10), 102241.
- 7 B. D. Conduit, T. Illston, S. Baker, D. V. Duggappa, S. Harding, H. J. Stone, *et al.*, Probabilistic neural network identification of an alloy for direct laser deposition, *Mater. Des.*, 2019, **168**, 107644.
- 8 T. A. Mansouri, A. O. Oliynyk, M. Parry, Z. Rizvi, S. Couper, F. Lin, *et al.*, Machine Learning Directed Search for Ultraincompressible, Superhard Materials, *J. Am. Chem. Soc.*, 2018, **140**(31), 9844–9853.
- 9 J. Schrier, A. J. Norquist, T. Buonassisi and J. Brgoch, In Pursuit of the Exceptional: Research Directions for Machine Learning in Chemical and Materials Science, *J. Am. Chem. Soc.*, 2023, **145**(40), 21699–21716.
- 10 A. Way, J. Luke, A. D. Evans, Z. Li, J. S. Kim, J. R. Durrant, *et al.*, Fluorine doped tin oxide as an alternative of indium tin oxide for bottom electrode of semi-transparent organic photovoltaic devices, *AIP Adv.*, 2019, **9**(8), 085220.
- 11 S. K. Maurya, H. R. Galvan, G. Gautam and X. Xu, Recent Progress in Transparent Conductive Materials for Photovoltaics, *Energies*, 2022, **15**(22), 8698.
- 12 M. Morales-Masis, S. De Wolf, R. Woods-Robinson, J. W. Ager and C. Ballif, Transparent Electrodes for Efficient Optoelectronics, *Adv. Electron. Mater.*, 2017, **3**(5), 1600529.
- 13 R. Woods-Robinson, D. Broberg, A. Faghaninia, A. Jain, S. S. Dwaraknath and K. A. Persson, Assessing High-Throughput Descriptors for Prediction of Transparent Conductors, *Chem. Mater.*, 2018, **30**(22), 8375–8389.
- 14 X. Xiong, Y. Sun, Y. Xing and T. Hato, *Investigate Machine Learning Methods for Transparent Conductors Prediction*, 2018, [http://noiselab.ucsd.edu/ECE228\\_2018/](http://noiselab.ucsd.edu/ECE228_2018/).
- 15 C. Sutton, C. Bartel, X. Liu, M. Boley, M. Rupp, L. Ghiringhelli, *et al.*, Evaluation of Machine Learning Methods for the Prediction of Key Properties for Novel Transparent Semiconductors, in *APS March Meeting Abstracts*, 2018, vol. 2018, p. E34.012.
- 16 P. Villars, K. Cenzual and W. B. Pearson, *Pearson's Crystal Data: Crystal Structure Database for Inorganic Compounds*, 2007.
- 17 D. Zagorac, H. Müller, S. Ruehl, J. Zagorac and S. Rehme, Recent developments in the Inorganic Crystal Structure Database: theoretical crystal structure data and related features, *J. Appl. Crystallogr.*, 2019, **52**(5), 918–925.
- 18 G. Hautier, A. Miglio, D. Waroquiers, G. M. Rignanese and X. Gonze, How Does Chemistry Influence Electron Effective Mass in Oxides? A High-Throughput Computational Analysis, *Chem. Mater.*, 2014, **26**(19), 5447–5458.
- 19 Y. Sun, Y. Xing, X. Xiong and T. Hao, *Investigate Machine Learning Methods for Transparent Conductors Prediction*, 2018, [http://noiselab.ucsd.edu/ECE228\\_2018/Reports/Report3.pdf](http://noiselab.ucsd.edu/ECE228_2018/Reports/Report3.pdf).
- 20 L. M. Antunes, V. Vikram, J. J. Plata, A. V. Powell, K. T. Butler and R. Grau-Crespo, Machine learning approaches for accelerating the discovery of thermoelectric materials, in *Machine Learning in Materials Informatics: Methods and Applications*, ACS Publications, 2022, pp. 1–32.
- 21 M. W. Gaultois, T. D. Sparks, C. K. H. Borg, R. Seshadri, W. D. Bonificio and D. R. Clarke, Data-Driven Review of Thermoelectric Materials: Performance and Resource Considerations, *Chem. Mater.*, 2013, **25**(15), 2911–2920.
- 22 Y. Zhuo, A. Mansouri Tehrani and J. Brgoch, Predicting the Band Gaps of Inorganic Solids by Machine Learning, *J. Phys. Chem. Lett.*, 2018, **9**(7), 1668–1673.
- 23 T. Wang, K. Zhang, J. Thé and H. Yu, Accurate prediction of band gap of materials using stacking machine learning model, *Comput. Mater. Sci.*, 2022, **201**, 110899.
- 24 M. Mukherjee, S. Satsangi and A. K. Singh, A Statistical Approach for the Rapid Prediction of Electron Relaxation Time Using Elemental Representatives, *Chem. Mater.*, 2020, **32**(15), 6507–6514.
- 25 G. S. Na, S. Jang and H. Chang, Predicting thermoelectric properties from chemical formula with explicitly identifying dopant effects, *npj Comput. Mater.*, 2021, **7**(1), 106.
- 26 F. Ricci, W. Chen, U. Aydemir, G. J. Snyder, G. M. Rignanese, A. Jain, *et al.*, An *ab initio* electronic transport database for inorganic materials, *Sci. Data*, 2017, **4**(1), 170085.
- 27 K. Choudhary, K. F. Garrity, A. C. E. Reid, B. DeCost, A. J. Bicchi, A. R. Hight Walker, *et al.*, The joint automated repository for various integrated simulations (JARVIS) for data-driven materials design, *npj Comput. Mater.*, 2020, **6**(1), 173.
- 28 M. Yao, Y. Wang, X. Li, Y. Sheng, H. Huo, L. Xi, *et al.*, Materials informatics platform with three dimensional structures, workflow and thermoelectric applications, *Sci. Data*, 2021, **8**(1), 236.
- 29 H. Miyazaki, T. Tamura, M. Mikami, K. Watanabe, N. Ide, O. M. Ozkendir, *et al.*, Machine learning based prediction of lattice thermal conductivity for half-Heusler compounds using atomic information, *Sci. Rep.*, 2021, **11**(1), 13410.
- 30 Y. Katsura, M. Kumagai, T. Kodani, M. Kaneshige, Y. Ando, S. Gunji, *et al.*, Data-driven analysis of electron relaxation times in PbTe-type thermoelectric materials, *Sci. Technol. Adv. Mater.*, 2019, **20**(1), 511–520.
- 31 P. Priya and N. R. Aluru, Accelerated design and discovery of perovskites with high conductivity for energy applications through machine learning, *npj Comput. Mater.*, 2021, **7**(1), 90.



- 32 G. S. Na and H. Chang, A public database of thermoelectric materials and system-identified material representation for data-driven discovery, *npj Comput. Mater.*, 2022, **8**(1), 214.
- 33 S. Curtarolo, W. Setyawan, G. L. W. Hart, M. Jahnatek, R. V. Chepulskii, R. H. Taylor, *et al.*, AFLOW: An automatic framework for high-throughput materials discovery, *Comput. Mater. Sci.*, 2012, **58**, 218–226.
- 34 A. J. Cohen, P. Mori-Sánchez and W. Yang, Insights into Current Limitations of Density Functional Theory, *Science*, 2008, **321**(5890), 792–794.
- 35 R. G. Gordon, Criteria for Choosing Transparent Conductors, *MRS Bull.*, 2000, **25**(8), 52–57.
- 36 J. Clymo, C. M. Collins, K. Atkinson, M. S. Dyer, M. W. Gaultois, V. V. Gusev, M. J. Rosseinsky and S. Schewe, Exploration of chemical space through automated reasoning, *Angew. Chem., Int. Ed.*, 2025, **64**(6), e202417657.
- 37 N. F. Mott, Is there ever a minimum metallic conductivity?, *Solid-State Electron.*, 1985, **28**(1), 57–59.
- 38 F. A. Chudnovskii, The minimum conductivity and electron localisation in the metallic phase of transition metal compounds in the vicinity of a metal-insulator transition, *J. Phys. C: Solid State Phys.*, 1978, **11**(3), L99.
- 39 A. Dunn, Q. Wang, A. Ganose, D. Dopp and A. Jain, Benchmarking materials property prediction methods: the Matbench test set and Automatminer reference algorithm, *npj Comput. Mater.*, 2020, **6**(1), 138.
- 40 J. Portier, G. Campet, C. W. Kwon, J. Etourneau and M. A. Subramanian, Relationships between optical band gap and thermodynamic properties of binary oxides, *Int. J. Inorg. Mater.*, 2001, **3**(7), 1091–1094.
- 41 F. Di Quarto, C. Sunseri, S. Piazza and M. C. Romano, Semiempirical Correlation between Optical Band Gap Values of Oxides and the Difference of Electronegativity of the Elements. Its Importance for a Quantitative Use of Photocurrent Spectroscopy in Corrosion Studies, *J. Phys. Chem. B*, 1997, **101**(14), 2519–2525.
- 42 B. Teldja, B. Noureddine, B. Azzeddine and T. Meriem, Effect of indium doping on the UV photoluminescence emission, structural, electrical and optical properties of spin-coating deposited SnO<sub>2</sub> thin films, *Optik*, 2020, **209**, 164586.
- 43 P. Sivakumar, H. S. Akkera, T. Ranjeth Kumar Reddy, G. Srinivas Reddy, N. Kambhala and N. Nanda Kumar Reddy, Influence of Ga doping on structural, optical and electrical properties of transparent conducting SnO<sub>2</sub> thin films, *Optik*, 2021, **226**, 165859.
- 44 I. Arora, K. Malhotra, A. Mahajan and P. Kumar, Structural, optical and electrical characterization of spin coated SnO<sub>2</sub>:Mn thin films, *Mater. Today: Proc.*, 2021, **36**, 697–700.
- 45 V. Uwhoreye, Z. Yang, J. Y. Zhang, Y. M. Lin, X. Liang, L. Yang, *et al.*, Transparent conductive SnO<sub>2</sub> thin films via resonant Ta doping, *Sci. China Mater.*, 2023, **66**(1), 264–271.
- 46 P. Sivakumar, H. S. Akkera, T. R. Kumar Reddy, Y. Bitla, V. Ganesh, P. M. Kumar, *et al.*, Effect of Ti doping on structural, optical and electrical properties of SnO<sub>2</sub> transparent conducting thin films deposited by sol-gel spin coating, *Opt. Mater.*, 2021, **113**, 110845.
- 47 M. Wang, Y. Gao, Z. Chen, C. Cao, J. Zhou, L. Dai, *et al.*, Transparent and conductive W-doped SnO<sub>2</sub> thin films fabricated by an aqueous solution process, *Thin Solid Films*, 2013, **544**, 419–426.
- 48 R. K. Shukla, A. Srivastava, A. Srivastava and K. C. Dubey, Growth of transparent conducting nanocrystalline Al doped ZnO thin films by pulsed laser deposition, *J. Cryst. Growth*, 2006, **294**(2), 427–431.
- 49 R. S. Ajimsha, A. K. Das, P. Misra, M. P. Joshi, L. M. Kukreja, R. Kumar, *et al.*, Observation of low resistivity and high mobility in Ga doped ZnO thin films grown by buffer assisted pulsed laser deposition, *J. Alloys Compd.*, 2015, **638**, 55–58.
- 50 L. Shen, Y. An, R. Zhang, P. Zhang, Z. Wu, H. Yan, *et al.*, Enhanced room-temperature ferromagnetism on (In<sub>0.98-x</sub>Co<sub>x</sub>Sn<sub>0.02</sub>)<sub>2</sub>O<sub>3</sub> films: magnetic mechanism, optical and transport properties, *Phys. Chem. Chem. Phys.*, 2017, **19**, 29472–29482.
- 51 H. R. Fallah, M. Ghasemi, A. Hassanzadeh and H. Steki, The effect of annealing on structural, electrical and optical properties of nanostructured ITO films prepared by e-beam evaporation, *Mater. Res. Bull.*, 2007, **42**(3), 487–496.
- 52 A. Ambrosini, A. Duarte, K. R. Poepelmeier, M. Lane, C. R. Kannewurf and T. O. Mason, Electrical, Optical, and Structural Properties of Tin-Doped In<sub>2</sub>O<sub>3</sub>-M<sub>2</sub>O<sub>3</sub> Solid Solutions (M=Y, Sc), *J. Solid State Chem.*, 2000, **153**(1), 41–47.
- 53 H. Guendouz, A. Bouaine and N. Brihi, Biphasic effect on structural, optical, and electrical properties of Al-Sn codoped ZnO thin films deposited by sol-gel spin-coating technique, *Optik*, 2018, **158**, 1342–1348.
- 54 L. Ward, A. Agrawal, A. Choudhary and C. Wolverton, A general-purpose machine learning framework for predicting properties of inorganic materials, *npj Comput. Mater.*, 2016, **2**(1), 16028.
- 55 V. Tshitoyan, J. Dagdelen, L. Weston, A. Dunn, Z. Rong, O. Kononova, *et al.*, Unsupervised word embeddings capture latent knowledge from materials science literature, *Nature*, 2019, **571**(7763), 95–98.
- 56 A. Y. T. Wang, S. K. Kauwe, R. J. Murdock and T. D. Sparks, Compositionally restricted attention-based network for materials property predictions, *npj Comput. Mater.*, 2021, **7**(1), 77.
- 57 R. E. A. Goodall and A. A. Lee, Predicting materials properties without crystal structure: deep representation learning from stoichiometry, *Nat. Commun.*, 2020, **11**(1), 6280.
- 58 L. Breiman, Random Forests, *Mach. Learn.*, 2001, **45**(1), 5–32.
- 59 V. Venkatraman, The utility of composition-based machine learning models for band gap prediction, *Comput. Mater. Sci.*, 2021, **197**, 110637.
- 60 J. Riebesell, Probabilistic Data-Driven Discovery of Thermoelectric Materials, MPhil thesis, University of Cambridge, 2019, <https://github.com/janosh/thermo>.



- 61 S. J. S. Chelladurai, K. Upreti, M. Verma, M. Agrawal, J. Garg, R. Kaushik, *et al.*, Prediction of Mechanical Strength by Using an Artificial Neural Network and Random Forest Algorithm, *J. Nanomater.*, 2022, **2022**, 7791582.
- 62 A. Sonpal, M. A. F. Afzal, Y. An, A. Chandrasekaran and M. D. Halls, *Benchmarking Machine Learning Descriptors for Crystals*, American Chemical Society, 2022. vol. 1416 of ACS Symposium Series, pp. 111–126.
- 63 A. Vaswani, N. Shazeer, N. Parmar, J. Uszkoreit, L. Jones, A. N. Gomez, *et al.*, Attention is All you Need, in *Advances in Neural Information Processing Systems*, ed. I. Guyon, U. V. Luxburg, S. Bengio, H. Wallach, R. Fergus, S. Vishwanathan, *et al.*, Curran Associates, Inc., 2017, vol. 30, <https://proceedings.neurips.cc/paper/2017/file/3f5ee243547dee91fbd053c1c4a845aa-Paper.pdf>.
- 64 S. G. Baird, T. Q. Diep and T. D. Sparks, DiSCoVeR: a materials discovery screening tool for high performance, unique chemical compositions, *Digital Discovery*, 2022, **1**, 226–240.
- 65 C. J. Hargreaves, M. W. Gaultois, L. M. Daniels, E. J. Watts, V. A. Kurlin, M. Moran, *et al.*, A database of experimentally measured lithium solid electrolyte conductivities evaluated with machine learning, *npj Comput. Mater.*, 2023, **9**(1), 9.
- 66 L. M. Antunes, K. T. Butler and R. Grau-Crespo, Predicting thermoelectric transport properties from composition with attention-based deep learning, *Mach. Learn.: Sci. Technol.*, 2023, **4**(1), 015037.
- 67 J. Lee, C. Park, H. Yang, S. Han and W. Lim, CLCS: Contrastive Learning between Compositions and Structures for practical Li-ion battery electrodes design, in *AI for Accelerated Materials Design – NeurIPS 2023 Workshop*, 2023, <https://openreview.net/forum?id=FfvByoVAO>.
- 68 T. Nguyen-Sy, Q. D. To, M. N. Vu, T. D. Nguyen and T. T. Nguyen, Predicting the electrical conductivity of brine-saturated rocks using machine learning methods, *J. Appl. Geophys.*, 2021, **184**, 104238.
- 69 T. Hastie, R. Tibshirani and J. Friedman, *The Elements of Statistical Learning*, *Springer Series in Statistics*, Springer New York Inc., New York, NY, USA, 2001.
- 70 B. Meredig, E. Antono, C. Church, M. Hutchinson, J. Ling, S. Paradiso, *et al.*, Can machine learning identify the next high-temperature superconductor? Examining extrapolation performance for materials discovery, *Mol. Syst. Des. Eng.*, 2018, **3**, 819–825.
- 71 F. Ottomano, G. De Felice, V. V. Gusev and T. D. Sparks, Not as simple as we thought: a rigorous examination of data aggregation in materials informatics, *Digital Discovery*, 2024, **3**(2), 337–346.
- 72 K. Li, B. DeCost, K. Choudhary, M. Greenwood and J. Hatrick-Simpers, A critical examination of robustness and generalizability of machine learning prediction of materials properties, *npj Comput. Mater.*, 2023, **9**(1), 55.
- 73 S. S. Omeel, N. Fu, R. Dong, M. Hu and J. Hu, Structure-based out-of-distribution (OOD) materials property prediction: a benchmark study, *npj Comput. Mater.*, 2024, **10**(1), 144.
- 74 S. P. Lloyd, Least squares quantization in PCM, *IEEE Trans. Inf. Theory*, 1982, **28**, 129–136.
- 75 S. Durdy, M. W. Gaultois, V. V. Gusev, D. Bollegala and M. J. Rosseinsky, Random projections and kernelised leave one cluster out cross validation: universal baselines and evaluation tools for supervised machine learning of material properties, *Digital Discovery*, 2022, **1**, 763–778.
- 76 T. Hofmann, B. Schölkopf and A. J. Smola, Kernel methods in machine learning, *Ann. Stat.*, 2008, **36**(3), 1171–1220.
- 77 N. Shoghi, A. Kolluru, J. R. Kitchin, Z. W. Ulissi, C. L. Zitnick and B. M. Wood, *From Molecules to Materials: Pre-training Large Generalizable Models for Atomic Property Prediction*, 2023.
- 78 K. Jablonka, P. Schwaller, A. Ortega-Guerrero and B. Smit, Leveraging large language models for predictive chemistry, *Nat. Mach. Intell.*, 2024, **6**, 1–9.
- 79 D. Chicco and G. Jurman, The advantages of the Matthews correlation coefficient (MCC) over F1 score and accuracy in binary classification evaluation, *BMC Genomics*, 2020, **21**(1), 6.
- 80 P. Linardatos, V. Papastefanopoulos and S. Kotsiantis, Explainable AI: A Review of Machine Learning Interpretability Methods, *Entropy*, 2021, **23**(1), 18.
- 81 Y. Michiue, H. W. Son and T. Mori, Utilizing a unified structure model in (3+1)-dimensional superspace to identify a homologous phase (Ga<sub>1-α</sub>Al<sub>α</sub>)<sub>2</sub>O<sub>3</sub>(ZnO)<sub>m</sub> in ZnO-based thermoelectric composites, *J. Appl. Crystallogr.*, 2020, **53**(6), 1542–1549.
- 82 N. Erdogan, T. Kutlu, N. Sedefoglu and H. Kavak, Effect of Na doping on microstructures, optical and electrical properties of ZnO thin films grown by sol-gel method, *J. Alloys Compd.*, 2021, **553**, 160554.
- 83 H. Mahdhi, K. Djessas and Z. B. Ayadi, Synthesis and characteristics of Ca-doped ZnO thin films by rf magnetron sputtering at low temperature, *Mater. Lett.*, 2018, **214**, 10–14.
- 84 A. Dolgonos, S. A. Wells, K. R. Poeppelmeier and T. O. Mason, Phase stability and optoelectronic properties of the bixbyite phase in the gallium-indium-tin-oxide system, *J. Am. Ceram. Soc.*, 2015, **98**(2), 669–674.
- 85 A. Ahmad, M. Umer, X. Tan, R. Liu, F. Mohamad, M. Hussain, G. K. Ren and Y. H. Lin, High-temperature electrical and thermal transport behaviors of In<sub>2</sub>O<sub>3</sub>-based ceramics by Zn–Sn co-substitution, *J. Appl. Phys.*, 2018, **123**(24), 245108.
- 86 R. K. Sahu, R. Vispute, S. Dhar, D. Kundaliya, S. S. Manoharan, T. Venkatesan, *et al.*, Enhanced conductivity of pulsed laser deposited n-InGaZn<sub>6</sub>O<sub>9</sub> films and its rectifying characteristics with p-SiC, *Thin Solid Films*, 2009, **517**(5), 1829–1832.
- 87 S. Préaud, C. Byl, F. Brisset and D. Berardan, SPS-assisted synthesis of InGaO<sub>3</sub> (ZnO) m ceramics, and influence of m on the band gap and the thermal conductivity, *J. Am. Ceram. Soc.*, 2020, **103**(5), 3030–3038.



- 88 Y. S. Lee, C. H. Chang, Y. C. Lin, R. J. Lyu, H. C. Lin and T. Y. Huang, Effects of Ga<sub>2</sub>O<sub>3</sub> deposition power on electrical properties of cosputtered In-Ga-Zn-O semiconductor films and thin-film transistors, *Jpn. J. Appl. Phys.*, 2014, **53**(5S3), 05HA02.
- 89 M. Nakamura, N. Kimizuka and T. Mohri, The phase relations in the In<sub>2</sub>O<sub>3</sub>-Ga<sub>2</sub>ZnO<sub>4</sub>-ZnO system at 1350 °C, *J. Solid State Chem.*, 1991, **93**(2), 298–315.
- 90 A. Suresh, P. Gollakota, P. Wellenius, A. Dhawan and J. F. Muth, Transparent, high mobility InGaZnO thin films deposited by PLD, *Thin Solid Films*, 2008, **516**(7), 1326–1329.
- 91 H. Jung, Y. Park, S. Gedi, V. R. M. Reddy, G. Ferblantier and W. K. Kim, Al-doped zinc stannate films for photovoltaic applications, *Korean J. Chem. Eng.*, 2020, **37**, 730–735.
- 92 M. Orita, H. Ohta, M. Hirano, S. Narushima and H. Hosono, Amorphous transparent conductive oxide InGaO<sub>3</sub> (ZnO) m (mle 4): a Zn<sub>4</sub>s conductor, *Philos. Mag. B*, 2001, **81**(5), 501–515.
- 93 E. S. Anannikov, T. A. Markin, I. A. Solizoda, G. M. Zirnik, D. A. Uchaev, A. S. Chernukha, *et al.*, Synthesis and research of physical and chemical properties of InGaZn<sub>2</sub>O<sub>5</sub> prepared by nitrate-glycolate gel decomposition method. *Nanosystems: Physics, Chemistry, Mathematics*, 2024, **15**(6), 806–813.
- 94 K. Rickert, A. Huq, S. H. Lapidus, A. Wustrow, D. E. Ellis and K. R. Poeppelmeier, Site Dependency of the High Conductivity of Ga<sub>2</sub>In<sub>6</sub>Sn<sub>2</sub>O<sub>16</sub>: The Role of the 7-Coordinate Site, *Chem. Mater.*, 2015, **27**(23), 8084–8093.
- 95 Q. Li, L. Zhang, C. Tang, P. Zhao, C. Yin and J. Yin, Synthesis of Zn (In<sub>x</sub>Ga<sub>1-x</sub>)<sub>2</sub>O<sub>4</sub> solid-solutions with tunable band-gaps for enhanced photocatalytic hydrogen evolution under solar-light irradiation, *Int. J. Hydrogen Energy*, 2020, **45**(11), 6621–6628.
- 96 J. Rezek, J. Houška, M. Procházká, S. Haviar, T. Kozák and P. Baroch, In-Ga-Zn-O thin films with tunable optical and electrical properties prepared by high-power impulse magnetron sputtering, *Thin Solid Films*, 2018, **658**, 27–32.
- 97 J. Grover, S. Arrasmith and D. D. Edwards, Thermoelectric properties and impedance spectroscopy of polycrystalline samples of the beta-gallia rutile intergrowth, (Ga,In)<sub>4</sub>(Sn,Ti)<sub>5</sub>O<sub>16</sub>, *J. Solid State Chem.*, 2012, **191**, 129–135.
- 98 E. Finley and J. Brgoch, Deciphering the loss of persistent red luminescence in ZnGa<sub>2</sub>O<sub>4</sub>: Cr<sup>3+</sup> upon Al<sup>3+</sup> substitution, *J. Mater. Chem. C*, 2019, **7**(7), 2005–2013.
- 99 D. Edwards, T. Mason, F. Goutenoire and K. Poeppelmeier, A new transparent conducting oxide in the Ga<sub>2</sub>O<sub>3</sub>-In<sub>2</sub>O<sub>3</sub>-SnO<sub>2</sub> system, *Appl. Phys. Lett.*, 1997, **70**(13), 1706–1708.
- 100 K. Sakoda and M. Hirano, Formation of complete solid solutions, Zn(Al<sub>x</sub>Ga<sub>1-x</sub>)<sub>2</sub>O<sub>4</sub> spinel nanocrystals *via* hydrothermal route, *Ceram. Int.*, 2014, **40**(10), 15841–15848.
- 101 M. A. Basyooni, M. Shaban and A. M. El Sayed, Enhanced gas sensing properties of spin-coated Na-doped ZnO nanostructured films, *Sci. Rep.*, 2017, **7**(1), 41716.
- 102 D. D. Edwards and T. O. Mason, Subsolidus Phase Relations in the Ga<sub>2</sub>O<sub>3</sub>-In<sub>2</sub>O<sub>3</sub>-SnO<sub>2</sub> System, *J. Am. Ceram. Soc.*, 1998, **81**(12), 3285–3292.
- 103 M. Orita, H. Tanji, M. Mizuno, H. Adachi and I. Tanaka, Mechanism of electrical conductivity of transparent InGaZnO<sub>4</sub>, *Phys. Rev. B: Condens. Matter Mater. Phys.*, 2000, **61**(3), 1811.
- 104 A. Murat, A. U. Adler, T. O. Mason and J. E. Medvedeva, Carrier generation in multicomponent wide-bandgap oxides: InGaZnO<sub>4</sub>, *J. Am. Chem. Soc.*, 2013, **135**(15), 5685–5692.
- 105 S. K. Kauwe, J. Graser, R. Murdock and T. D. Sparks, Can machine learning find extraordinary materials?, *Comput. Mater. Sci.*, 2020, **174**, 109498.
- 106 T. Xie, Y. Wan, Y. Zhou, W. Huang, Y. Liu, Q. Linghu, *et al.*, *Large Language Models as Master Key: Unlocking the Secrets of Materials Science*, 2023.
- 107 N. Lee, H. Noh, G. S. Na, T. Fu, J. Sun and C. Park, Stoichiometry Representation Learning with Polymorphic Crystal Structures, *arXiv*, 2023, preprint, arXiv:2312.13289, DOI: [10.48550/arXiv.2312.13289](https://doi.org/10.48550/arXiv.2312.13289).

